Please cite this article in press as: DurieLin et al., Hsp104 and Potentiated Variants Can Operate as Distinct Nonprocessive Translocases, Biophysical Journal (2019), https://doi.org/10.1016/j.bpj.2019.03.035

Biophysical *Journal*
Article

Biophysical Society

Hsp104 and Potentiated Variants Can Operate as Distinct Nonprocessive Translocases

Clarissa L. Durie,[1] JiaBei Lin,[2] Nathaniel W. Scull,[1] Korrie L. Mack,[2] Meredith E. Jackrel,[2] Elizabeth A. Sweeny,[2] Laura M. Castellano,[2] James Shorter,[2] and Aaron L. Lucius[1,*]

[1]University of Alabama at Birmingham, Chemistry Department, Birmingham, Alabama and [2]Department of Biochemistry and Biophysics, Perelman School of Medicine at the University of Pennsylvania, Philadelphia, Pennsylvania

ABSTRACT Heat shock protein (Hsp) 104 is a hexameric ATPases associated with diverse cellular activities motor protein that enables cells to survive extreme stress. Hsp104 couples the energy of ATP binding and hydrolysis to solubilize proteins trapped in aggregated structures. The mechanism by which Hsp104 disaggregates proteins is not completely understood but may require Hsp104 to partially or completely translocate polypeptides across its central channel. Here, we apply transient state, single turnover kinetics to investigate the ATP-dependent translocation of soluble polypeptides by Hsp104 and Hsp104^{A503S}, a potentiated variant developed to resolve misfolded conformers implicated in neurodegenerative disease. We establish that Hsp104 and Hsp104^{A503S} can operate as nonprocessive translocases for soluble substrates, indicating a "partial threading" model of translocation. Remarkably, Hsp104^{A503S} exhibits altered coupling of ATP binding to translocation and decelerated dissociation from polypeptide substrate compared to Hsp104. This altered coupling and prolonged substrate interaction likely increases entropic pulling forces, thereby enabling more effective aggregate dissolution by Hsp104^{A503S}.

INTRODUCTION

Heat shock protein (Hsp) 104 rescues damaged proteins from aggregates, helping organisms survive and adapt to environmental stresses (1,2). A member of the ATPases associated with diverse cellular activities (AAA+) protein family, Hsp104 uses the energy of ATP binding and hydrolysis to perform mechanical work (3). Hsp104 and its homologs are conserved through bacteria, fungi, protozoa, algae, and plants, but no such homolog exists in the cytosol of animal cells (4,5). Because protein aggregates and toxic soluble oligomers are implicated in many neurodegenerative diseases, there is interest in developing therapeutic forms of Hsp104 that can safely dissociate soluble toxic oligomers and reverse aggregation associated with neurodegenerative diseases (6). Recently, potentiated variants of yeast Hsp104 were shown to rescue yeast, *Caenorhabditis elegans*, and mammalian cell models of human neurodegenerative diseases (7–9). However, many questions remain open regarding how, at the molecular level, both the wild-type (WT) disaggregase and potentiated variants catalyze protein disaggregation.

A "complete threading" translocation mechanism is often advanced as describing Hsp104-catalyzed protein disaggregation. In this model, ATP binding and hydrolysis are coupled to translocating the entire polypeptide across the axial channel (10,11). This model is based largely on structural similarities between Hsp104 and *Escherichia coli* ClpA, another Hsp100 and AAA+ family member that also works in protein-quality control (4). ClpA couples the energy from ATP binding and hydrolysis to processive translocation of proteins through the axial channel of the ClpA homohexameric ring into the proteolytic partner protein ClpP (12–16).

Notably, although Hsp104 has been connected to the degradation of select substrates (17,18), it typically promotes protein solubilization and not degradation (1,19) and, natively, is not able to bind ClpP (20). Experimental evidence in support of a complete threading model for Hsp104 comes largely from an engineered interaction with ClpP. Hsp104 can be engineered to interact with ClpP by introducing three mutations (G739I:S740G:K741F) based on ClpA into a helix-loop-helix motif (20). The resulting Hsp104 variant, termed HAP, is able to promote the

Submitted October 17, 2018, and accepted for publication March 25, 2019.

*Correspondence: allucius@uab.edu

Clarissa L. Durie's present address is Life Sciences Institute, University of Michigan, Ann Arbor, Michigan.

Meredith E. Jackrel's present address is Department of Chemistry, Washington University, St. Louis, St. Louis, Missouri.

Elizabeth A. Sweeny's present address is Department of Pathobiology, Lerner Research Institute, Cleveland Clinic, Cleveland, Ohio.

Editor: Enrique De La Cruz.

https://doi.org/10.1016/j.bpj.2019.03.035

Please cite this article in press as: DurieLin et al., Hsp104 and Potentiated Variants Can Operate as Distinct Nonprocessive Translocases, Biophysical Journal (2019), https://doi.org/10.1016/j.bpj.2019.03.035

degradation of soluble and aggregated polypeptides in the presence of ClpP, including stable amyloid fibrils (20,21). These findings are consistent with complete translocation. However, studies with the *E. coli* ClpB version of HAP, termed BAP (in which S722-N748 of ClpB are replaced with V609-I635 of ClpA (22)), indicate that BAP-ClpP can degrade substrates in an ATP-independent manner (23). Thus, it continues to remain uncertain whether ClpB catalyzes processive translocation of the protein substrate driven by ATP hydrolysis.

Recent high-resolution structural data has also been interpreted in the context of a threading model (24,25). Cryogenic electron microscopy (Cryo-EM) reconstructions have revealed Hsp104 in closed and extended right-handed spiral states bound to casein in the presence of ATPγS as well as in left-handed open "lock-washer" states in the presence of adenylyl-imidodiphosphate or ADP and the absence of a protein substrate (24,25). By morphing these images, a ratcheting mechanism of polypeptide translocation was proposed (24,25). A conformational switch from the open to closed state is proposed to bring polypeptide into the channel in an ATP hydrolysis-independent step, thereafter the hexamer might switch between successive, energy driven, closed and extended states to further translocate polypeptide processively into the Hsp104 channel (24,25). Consistently, in other studies, ClpB or an ATPase-dead variant of BAP, $BAP^{E279A/E678A}$, was observed with casein deep (~70–80 Å) in the axial channel (26,27). This observation suggests that, at least in the case of BAP, ATP hydrolysis is not required for engaging the substrate into the channel. However, this observation is not sufficient to support that casein is deeply "translocated" into the central pore. Another possibility is that the hexameric ring binds by wrapping around the protein substrate, resulting in the substrate deep within the axial channel without ATP-dependent translocation. Here, we seek to test the mechanism by which Hsp104 and potentiated variants translocate substrates, in solution, using transient state kinetic techniques.

Though "complete threading" and "partial threading" are commonly used in describing the unfolding, disaggregating, or translocating activities of Hsp104, how these descriptions might relate to processivity is uncertain. Here, we will use a mathematical definition of processivity (28). We define processivity as the probability that the enzyme will either step forward with translocation rate constant k_t or dissociate with dissociation rate constant k_d. This definition is illustrated in Eq. 1 for an arbitrary enzyme-substrate complex, *ES*, proceeding forward with rate constant k_t to form the first translocation intermediate, I_1, or dissociate with rate constant k_d into free enzyme, *E*, and free substrate, *S*. For a highly processive enzyme, this cycle would repeat multiple times before reaching the end of the lattice, assuming the lattice is much longer than the step size.

$$\begin{array}{l} ES \overset{k_t}{\rightarrow} I_1 \\ k_d \downarrow \\ E + S \end{array} \tag{1}$$

The processivity is mathematically defined by Eq. 2

$$\mathrm{Pr} = \frac{k_t}{k_t + k_d}, \tag{2}$$

where *Pr* is processivity, and k_t and k_d are defined above. As k_d approaches zero, processivity approaches unity. This case would describe an infinitely processive enzyme, again assuming the lattice is much longer than the step size, thereby allowing for the possibility of multiple steps (12,29,30). In contrast, as k_d exceeds k_t, then *Pr* approaches zero, describing a distributive enzyme. Thus, the processivity, *Pr*, as defined by Eq. 2 is a probability that varies between zero and one. Processivity can also be defined as the average number of lattice elements translocated per binding event. For a protein translocase, the lattice element would be amino acids. The probability processivity, *Pr*, can be related to a processivity, *N*, expressed as the average number of amino acids translocated per binding event through Eq. 3,

$$\mathrm{Pr} = \frac{k_t}{k_t + k_d} = e^{(-m/N)}, \tag{3}$$

where *m* represents the step size as the distance translocated in amino acids per step. With these definitions in mind, the model that Hsp104 completely threads a polypeptide chain through its axial channel is regarded as indicating a processive enzyme.

The "complete threading" model was widely accepted for the bacterial homolog of Hsp104, *E. coli* ClpB. Like Hsp104, ClpB has a high structural similarity with ClpA. Thus, Bukau and co-workers (22) employed a similar protein-engineering strategy to observe substrate degradation by a variant of ClpB, termed BAP (ClpB with ClpA's P-loop). In this construct, ClpB S722-N748 was replaced with V609-I635 of ClpA, thereby engineering ClpB to bind the protease ClpP (22,31). Recent transient state kinetic analysis of ClpB-catalyzed, ATP-dependent translocation of a polypeptide substrate revealed, however, that ClpB is a nonprocessive polypeptide translocase (23). Rather than completely threading an entire polypeptide chain through its axial channel, ClpB was observed to take only one or two kinetic steps on a polypeptide substrate independent of the length of the polypeptide chain. Using Eq. 3 with $N = 1$ m or $N = 2$ m predicts a processivity $Pr = 0.37$ and 0.61 for one step or two steps, respectively. This led us to propose a "tug and release" mechanism by which ClpB can resolve an aggregate by taking one or two translocation steps before dissociation and subsequent rebinding to repeat the cycle (23).

Please cite this article in press as: DurieLin et al., Hsp104 and Potentiated Variants Can Operate as Distinct Nonprocessive Translocases, Biophysical Journal (2019), https://doi.org/10.1016/j.bpj.2019.03.035

Consistent with this conclusion, ClpB and Hsp104 have been reported to use a "partial threading" mechanism to disaggregate some substrates (32). Moreover, Hsp104 employs a partial translocation mechanism to dissolve Sup35 prions (3,33). Thus, an open question is whether Hsp104 and ClpB typically disaggregate substrates via processive or nonprocessive translocation or via both mechanisms.

Here, we test predictions of the recent high-resolution structural investigation of Hsp104 and its translocation mechanism. To do so, we conduct an in solution investigation of the Hsp104 mechanism of ATP-dependent polypeptide translocation. Furthermore, to better understand how translocation and disaggregation are coupled, we investigate how the mechanism of the potentiated variant Hsp104^{A503S} differs from Hsp104. Using soluble polypeptide substrates, we establish that Hsp104 and Hsp104^{A503S} proceed through only one or two kinetic steps before dissociation from the soluble polypeptide chain, independent of chain length. This observation is inconsistent with "complete threading" by taking many steps of a small size (e.g., two amino acids) or highly processive translocation of the soluble polypeptide chain. Strikingly, however, we observe that the A503S mutation in the middle domain of Hsp104 alters the coupling of ATP binding to the observed translocation steps. Indeed, Hsp104^{A503S} exhibits decelerated dissociation from soluble polypeptide substrate compared to Hsp104. This altered mode of translocation likely increases entropic pulling forces, thereby enabling more effective aggregate dissolution by Hsp104^{A503S}.

METHODS

Buffers and reagents

All buffers were prepared with distilled, deionized water from a Purelab Ultra Genetic system (Evoqua Water Technologies, Warrendale, PA). All chemicals were reagent grade. ATPγS was purchased from Calbiochem (La Jolla, CA).

All experiments were performed in buffer HK150. Buffer HK150 contains 25 mM HEPES, 150 mM KCl, 10 mM $MgCl_2$, 2 mM dithiothreitol, and 10% glycerol (v/v) with pH 7.5 at 25°C.

Proteins and peptides

Hsp104 and Hsp104^{A503S} were prepared as previously described (7,34,35). The concentration of Hsp104 was determined at 280 nm in HK150 using the extinction coefficient $\varepsilon = 32{,}500\ M^{-1}cm^{-1}$, determined following the method of Edelhoch (36,37). All protein concentrations are reported in monomer units.

RepA truncation peptides were prepared by CPC Scientific (Sunnyvale, CA). The peptides are made of the first 30, 40, or 50 amino acids of the N-terminal sequence of RepA, with a cysteine residue added to either the N- or C-terminus for labeling. Labeling with fluorescein-5-maleimide was performed as previously described, forming a covalent bond between the peptide and the fluorophore (38). αS1-casein truncation peptides were prepared and labeled with fluorescein as previously described (39).

Steady-state fluorescence quenching control

Total fluorescence of $RepA_{1-30Flu}$ (100 nM final concentration) was observed in a Fluorolog-3 spectrophotometer (HORIBA Jobin Yvon, Edison, NJ) at 25°C. Fluorescence was excited at 494 nm, and emission was collected from 500 to 600 nm. ATPγS was added (final concentration of 300 μM) and allowed to incubate for ~20 min, after which time, an emission spectrum was collected. Finally, Hsp104 (final concentration of 2 μM) was then added and allowed to incubate for 20 min, and another fluorescence emission spectrum was collected. Upon the addition of each component, fluorescence cuvettes were gently inverted to mix the reaction solution. All reagents were equilibrated to 25°C for approximately 1 h before addition to the fluorescence cuvette. Simultaneous anisotropy and total fluorescence measurements were also collected (with excitation at 494 nm and emission at 515 nm) to confirm that fluorescence quenching was due to binding of $RepA_{1-30Flu}$ by Hsp104 in the presence of ATPγS (data not shown).

Rapid mixing experiments with fluorescein-modified RepA truncation peptides

All rapid mixing experiments were performed using an Applied Photophysics SX20 stopped-flow fluorometer. Fluorescence of fluorescein-modified peptides were excited at 494 nm and observed using a 515 nm cutoff long pass filter. All solutions were incubated for 1 h at 25°C before mixing. The syringes of the stopped-flow fluorimeter and the reaction cell were also maintained at 25°C. For each concentration of ATP, a minimum of six shots or pushes were collected and averaged. Each time course was at least five half-lives of the slowest kinetic step.

Substrate length dependence

One syringe of the stopped-flow fluorometer contained a solution of RepA peptide (100 nM), Hsp104 (2 μM), and ATPγS (300 μM). The other syringe contained a solution of 10 mM ATP and 20 μM α-casein. The solutions were loaded, separately, into the stopped-flow fluorimeter. The solutions were rapidly mixed. Each experiment was performed in triplicate. Experiments were conducted in the same manner for Hsp104^{A503S}, except that only NCys-labeled RepA peptides were used.

[ATP] dependence

A solution of $RepA_{Flu1-50}$ (20 nM), Hsp104 (2 μM), and ATPγS (300 μM) was incubated in one syringe of the stopped-flow fluorimeter. A solution of ATP (various concentrations) and 20 μM α-casein was incubated in the other syringe. The solutions were rapidly mixed. Each experiment was performed in triplicate.

Rapid mixing experiments with fluorescein-modified α-casein truncation peptides

Experiments were performed using an Applied Photophysics SX20 stopped-flow fluorometer as described above with the additional use of the Fluorescence Polarization Accessory. Two R-6095 photomultiplier tubes were used, each with a 515 nm cutoff long pass filter. One syringe of the stopped-flow fluorometer contained a solution of fluorescein-labeled α-casein peptide (20 nM), Hsp104 (2 μM), and ATPγS (300 μM). The other syringe contained a solution of 10 mM ATP and 20 μM α-casein. The solutions were loaded, separately, into the stopped-flow fluorimeter. The solutions were rapidly mixed. Experiments were replicated.

Nonlinear least squares analysis of transient state kinetics

See supplemental NLLS Analysis of Transient State Kinetics for derivations pertaining to the models used for data analysis.

Please cite this article in press as: DurieLin et al., Hsp104 and Potentiated Variants Can Operate as Distinct Nonprocessive Translocases, Biophysical Journal (2019), https://doi.org/10.1016/j.bpj.2019.03.035

RESULTS

Experimental logic and design

Recent structural data resulted in the proposal of a processive rotary translocation, or ratcheting, mechanism for Hsp104-catalyzed translocation of peptide substrate. In this model, conformational changes in Hsp104 protomers are coupled to ATP binding and hydrolysis. These conformational changes were proposed to advance the interactions between the pore loops of the Hsp104 hexamer and the engaged peptide by two amino acids per step. In this model, the movement of the peptide proceeds from Hsp104 nucleotide-binding domain (NBD) 1 to NBD2 (25).

Here, we test the proposed structure-based model using transient state kinetics. The experiments presented here are specifically designed to determine the number of ATP-driven steps the disaggregase takes before dissociation from the model polypeptide chain. In this approach, we use stopped-flow fluorescence to monitor the ATP-dependent peptide translocation and dissociation of Hsp104 as we have done with other AAA+ translocases (12,13,23).

Fig. 1 A is a schematic representation of Hsp104, and the primary structural features are labeled as the N-terminal domain, NBD1, middle domain, and NBD2. Fig. 1 B schematically depicts the method. In this design, Hsp104 is bound to a fluorescently labeled peptide (See Table 1) in the presence of ATPγS, where the ATPγS is included to

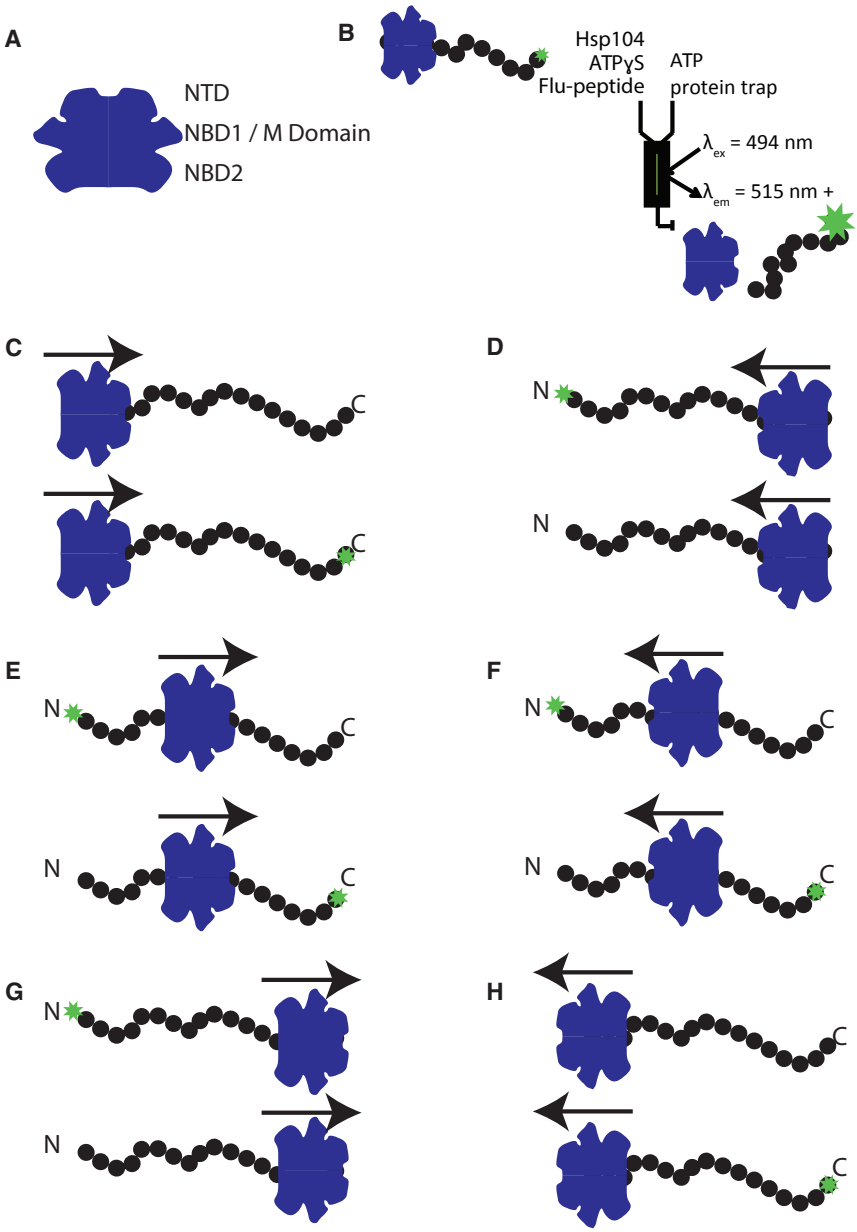

FIGURE 1 Possible orientations and directionality of Hsp104 on the peptide substrate. Hsp104 hexamers are depicted in blue from a side view. Peptides are depicted as linked black filled circles and the N- and C-termini are labeled. Green stars indicate a fluorescent dye covalently bound at either the N- or C-terminus of the peptide. (*A*) Identification of domain orientation is shown in the Hsp104 schematic. (*B*) Shown is a schematic for transient state, single turnover kinetic experiments. Hsp104, ATPγS, and fluorescently labeled peptide are incubated in one syringe, whereas ATP and α-casein are incubated in the other syringe of a stopped-flow fluorimeter at 25°C. The contents of the two syringes are rapidly mixed. The fluorescence is excited at 494 nm, and the emission is observed at 515 nm and above. (*C–H*) Shown are the possible orientations of the Hsp104-peptide complex formed in the presence of ATPγS. Arrow indicates the direction of the Hsp104 movement with respect to the peptide. Green star indicates the location of fluorescein dye on the peptide. To see this figure in color, go online.

Please cite this article in press as: DurieLin et al., Hsp104 and Potentiated Variants Can Operate as Distinct Nonprocessive Translocases, Biophysical Journal (2019), https://doi.org/10.1016/j.bpj.2019.03.035

TABLE 1 Polypeptide Substrates Used in This Study

Name	Length (aa)	Sequence
$RepA_{Flu1–30}$	30	Flu-C MNQSFISDIL YADIESKAKE LTVNSNNTVQ
$RepA_{Flu1–40}$	40	Flu-C MNQSFISDIL YADIESKAKE LTVNSNNTVQ PVALMRLGVF
$RepA_{Flu1–50}$	50	Flu-C MNQSFISDIL YADIESKAKE LTVNSNNTVQ PVALMRLGVF VPKPSKSKGE
$RepA_{1–30Flu}$	30	MNQSFISDIL YADIESKAKE LTVNSNNTVQ C-Flu
$RepA_{1–40Flu}$	40	MNQSFISDIL YADIESKAKE LTVNSNNTVQ PVALMRLGVF C-Flu
$RepA_{1–50Flu}$	50	MNQSFISDIL YADIESKAKE LTVNSNNTVQ PVALMRLGVF VPKPSKSKGE C-Flu
$casein_{Flu102}$	102	C-terminal 101 AA of aS1-casein with N-terminal cysteine
$casein_{Flu127}$	127	C-terminal 127 AA of aS1-casein with N-terminal cysteine
$casein_{127Flu}$	127	C-terminal 127 AA of aS1-casein with C-terminal cysteine

Flu, fluorescein dye covalently attached to the cysteine residue.

ensure avid binding to the polypeptide substrate (25,38). The preformed complex always exhibits a fluorescence quenching when Hsp104 is bound (Fig. S1) and, thus, a recovery in fluorescence when Hsp104 dissociates. This preformed and fluorescently quenched complex is rapidly mixed with ATP and a protein trap. In this experimental design, the hydrolysable ATP provides the energy for translocation, and the protein trap binds any Hsp104 not bound to the fluorescently labeled peptide or that dissociates from the polypeptide during or after translocation. The trap ensures that the signal reports on a single turnover of the Hsp104:Flu-peptide complex through multiple rounds of ATP binding and hydrolysis. It is important to note that we cannot distinguish between the dissociation of a hexamer as a single unit versus the dissociation through disassembly of the hexamer. However, the trap ensures that if dissociation is the result of disassembly, then reassembly on the polypeptide is not possible.

Although ATPγS will be slowly hydrolyzed by Hsp104 in the preincubation syringe, we have no evidence that this hydrolysis of ATPγS can be coupled to translocation beyond encapsulating substrate in the channel as observed via cryo-EM (25–27). Indeed, we observe no "shot-to-shot" variability over several hours, where shot-to-shot variability would indicate motor movement during the preincubation period (data not shown).

Simulated time courses for Hsp104-driven polypeptide translocation

It is unknown where Hsp104 binds on the polypeptides used in this study (see Table 1). Also unknown is the directionality of translocation relative to the C- or N-terminus of the polypeptide chain. However, the peptide is thought to enter the axial channel of Hsp104 at NBD1 and is translocated to NBD2 (Fig. 1 A) (25). Thus, the directionality with respect to Hsp104 is assumed to be from NBD1 to NBD2. However, it is unclear if the motor translocates from N- to C-terminus or from C- to N-terminus on the polypeptide lattice. Evidence from other substrates suggests that Hsp104 can translocate in either direction, from N- to C-terminus or from C- to N-terminus (40,41).

To simulate the expected signals from the kinetic time courses acquired from the stopped-flow experiment schematized in Fig. 1 B, we have schematized the potential sites on the polypeptide chain where Hsp104 can initiate translocation. Fig. 1 C assumes that the N-terminus of the polypeptide chain is bound by Hsp104, enters Hsp104 at NBD1, and is translocated toward NBD2. In contrast, Fig. 1 D assumes that the C-terminus of the peptide is bound by Hsp104, again entering from NBD1 of Hsp104. In both Fig. 1, C and D, the green star represents the position of the fluorophore, and when it is not visible, it is covered by Hsp104. Thus, the peptides are fluorescently modified at either the N- or C-terminus.

In the presence of ATPγS, based on the structural data, Hsp104 is initially bound to the polypeptide substrate in the closed conformation with 26 amino acids of the substrate already inside the axial channel (25). Upon the initiation of ATP-driven translocation, Hsp104 is proposed to step along the polypeptide chain with a step size of two amino acids per step (25). Our experimental design is not sensitive to the open conformation of the Hsp104 hexamer, which is not populated in the presence of ATPγS and polypeptide substrate (24,25).

With the above structural model in mind, we sought to simulate expected time courses for each of the potential starting positions and dye the positions indicated in Fig. 1, C–H. We consider representative possibilities in which Hsp104 translocates the entire length of a peptide substrate, some partial length of the peptide, or only the length of the peptide that is initially bound by the disaggregase.

In our method, we use a set of three polypeptides of length (L) 30, 40, and 50 amino acids. If Hsp104 is bound to either the N- or C-terminus as illustrated in Fig. 1, C and D, then 4, 14, and 24 amino acids would extend out of the axial channel (i.e., $L - 26$).

For Fig. 1, C and D, the structural model that proposed two amino acids per step predicts Hsp104 would take 15, 20, and 25 steps on the 30, 40, and 50 amino acid substrates, respectively, for complete translocation. The kinetic time courses that we predict for these three substrates for the binding conditions shown in Fig. 1, C and D are shown in Fig. S2 A. If Hsp104 is proceeding through ~15, 20, and 25 steps, the time courses are predicted to show a strong length dependence regardless of the position of the fluorescent probe because, in this assay, fluorescence is constant until dissociation.

Please cite this article in press as: DurieLin et al., Hsp104 and Potentiated Variants Can Operate as Distinct Nonprocessive Translocases, Biophysical Journal (2019), https://doi.org/10.1016/j.bpj.2019.03.035

Fig. 1, E and F illustrates the possibility that Hsp104 may bind in the middle of a polypeptide chain. As with binding at either the N- or C-terminus, the structural model predicts that, when bound in the middle, Hsp104 would still occlude 26 amino acids (25). In this case, the number of amino acids remaining outside of the channel on either end of the Hsp104 binding site would be fewer than when the disaggregase is bound to either the N- or C-terminus (i.e., 2, 7, and 12 amino acids for the 30, 40, and 50 amino acid substrates, respectively ($(L - 26)/2$)). Processive unidirectional translocation would then require the motor to translocate 28, 33, and 38 amino acids, respectively. Thus, for the binding condition illustrated by Fig. 1, E and F, we predict 14, 16.5, and 19 steps on the 30, 40, and 50 amino acid substrates, respectively. Fig. S2 B shows the predicted time courses for the 30, 40, and 50 amino acid substrates initiating ATP-driven translocation from the middle as illustrated in Fig. 1, E and F. Similar to binding at the end, the simulated time courses predict a clear substrate length dependence (Fig. S2 B).

Fig. 1, G and H illustrate Hsp104 binding to either the N- or C-terminus with the polypeptide extruding from the NBD2 side of the disaggregase. In this arrangement, Hsp104 would again occlude 26 amino acids and proceed through 13 steps with a two amino acid step size. However, because the disaggregase is bound to the end of the polypeptide and translocating the substrate from NBD1 to NBD2, we predict a length-independent lag. That is to say, regardless of substrate length, we predict that Hsp104 would take the same number of steps. Thus, the time course would exhibit a lag, which would be the same regardless of substrate length as illustrated in Fig. S2 C. However, this possibility does not agree with the Cryo-EM observation of substrate extending from the NBD1 end and not the NBD2 end of the Hsp104 hexamer (25). Note that recent CryoEM studies of ClpB and ATPase-dead BAP also revealed protein substrate occupancy in NBD1 but not NBD2 (26,27). Thus, although this possibility cannot be excluded, it is not supported by current structural data (25–27). If the CryoEM observations represent all possible arrangements of Hsp104 on substrate, then substrate extending only from NBD1 and not NBD2 must result from incomplete translocation.

It is also possible, perhaps even likely, that Hsp104 protein binds randomly along the polypeptide substrate. In other words, a stochastic distribution of the potential binding sites as illustrated in Fig. 1, C–H. This scenario would be identical to that of single-stranded DNA translocases that exhibit random binding along the nucleic acid (42,43). Length-dependent time courses are observed in an analogous single turnover experiment. From those simulations, we predict that if Hsp104 exhibits random binding along the polypeptide lattice, then we would again observe length-dependent time courses.

Experimental assessment of Hsp104-driven polypeptide translocation

To test the possibilities illustrated in Fig. 1, C–H, we performed single turnover polypeptide translocation experiments as illustrated in Fig. 1 B. Upon rapid mixing of the components, fluorescein is excited at 494 nm, and emission is observed at and above 515 nm (see Methods). As seen in Fig. 2 A, the initial fluorescence is low because of quenching in the bound complex (see Fig. S1 B) and increases over time as Hsp104 dissociates and the fluorescence quenching is relieved. This finding is consistent with observations from the same experimental design studying ClpA and ClpB (12,23,38) (see Fig. S3).

These experiments were carried out with 2 μM monomer Hsp104 and 100 nM peptide. Although this represents a 20-fold excess of Hsp104 monomers, the maximal amount of hexamer present and available to bind to the peptide is 333 nM. However, as we have previously shown, Hsp104 is in a dynamic equilibrium of hexamers and smaller oligomers (38). Thus, the actual concentration of hexamers is lower. We have performed experiments with 1 μM and 200 nM Hsp104, and the kinetic parameters are comparable (see Table S1).

Fig. 2 A (solid traces) displays representative time courses from the Hsp104-peptide complex prepared with $RepA_{Flu1–30}$, $RepA_{Flu1–40}$, and $RepA_{Flu1–50}$ (polypeptides summarized in Table 1). Strikingly, each time course exhibits a lag followed by an increase in signal. This lag indicates that more than one step with similar rate constants occur before dissociation from the polypeptide chain, which is consistent with ATP-driven translocation. Moreover, no lag was observed in identical experiments in which ATP was left out and those time courses proceeded on a longer timescale (see Fig. S3). The lag observed with Hsp104 contrasts with observations made with ClpB, which exhibits no lag before dissociation (23). If Hsp104 is a processive translocase ratcheting the polypeptide substrate through the axial channel with successive rounds of ATP hydrolysis, this lag is predicted to increase with increasing substrate length as shown in our simulations (Fig. 2, A and B) (12,13,29,30,44–47). However, Fig. 2 A shows that the extent of the lag is the same for all three polypeptide substrates ranging from 30 to 50 amino acids. This observation indicates that, regardless of length, Hsp104 dissociates after taking the same number of steps, which is inconsistent with a motor that completely threads a polypeptide chain through the axial channel by taking many steps of a small size (e.g., two amino acids). This observation may be consistent with the scenario depicted in Fig. 1, G and H in which Hsp104 binds at the end of the peptide substrate and translocates directly off that end, but this model appears inconsistent with available cryo-EM data (25).

The other prominent feature of the time courses in Fig. 2 A is that they are biphasic, which indicates that there are two

Please cite this article in press as: DurieLin et al., Hsp104 and Potentiated Variants Can Operate as Distinct Nonprocessive Translocases, Biophysical Journal (2019), https://doi.org/10.1016/j.bpj.2019.03.035

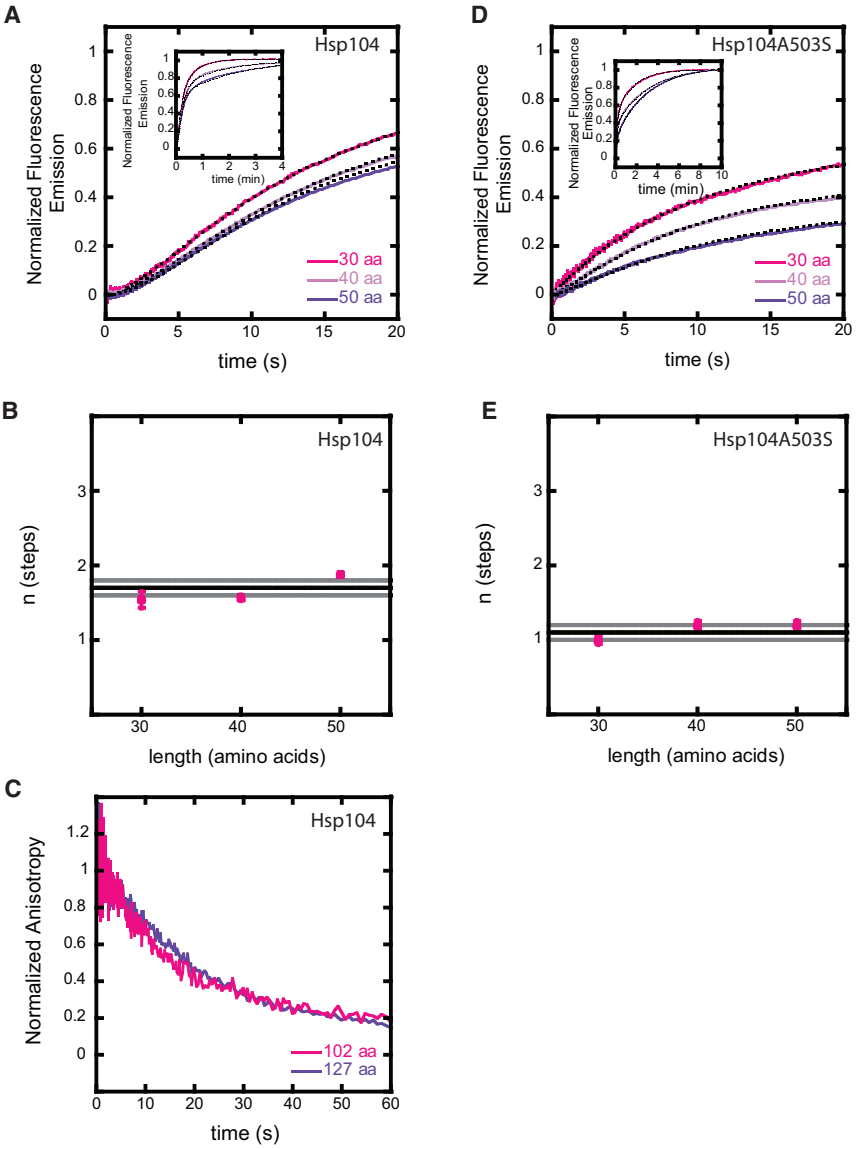

FIGURE 2 Substrate length independence. (*A*) Shown are the representative time courses from the rapid mixing of Hsp104 (2 μM), ATPγS (300 μM), and fluorescently labeled RepA truncation peptide (100 nM) against ATP (10 mM) and α-casein (20 μM). Colored traces are representative time courses using 30, 40, and 50 amino acid RepA truncation substrates labeled at the N-terminus. Inset shows the full time course for the inspection of the plateau region. Best fits from NLLS analysis of each time course, individually, to the equation derived from Eq. 4 are shown overlaid in black broken traces. Parameters are summarized in the first three rows of Table 2. (*B*) Shown is the number of repeating steps, n, as a function of substrate length. The average of three replicates of individual fits to Eq. 4 are shown (mean $\pm$ SE; n = 3). For all lengths, $n = (1.6 \pm 0.1)$ steps where the average is shown as a black line, and one SE in either direction is shown as a gray line. (*C*) Representative time courses of Hsp104 translocation and dissociation from N-terminally labeled 102 and 127 amino acid truncations of αS1-casein. Fluorescence is excited using polarized light at 494 nm, and fluorescence anisotropy is observed at 515 nm and above using a T format polarization accessory. (*D*) Shown is the representative time courses from assay as explained in (*A*) except with the potentiated variant Hsp104^{A503S}. (*E*) Shown is the number of repeating steps, n, as a function of substrate length for Hsp104^{A503S}. The average of three replicates of individual fits to Eq. 4 are shown (mean $\pm$ SE; n = 3). For all lengths, $n = (1.1 \pm 0.1)$ steps where the average is shown as a black line, and one SE in either direction is shown as a gray line. To see this figure in color, go online.

starting populations proceeding through the same kinetic path (29,30). The simplest mechanism that accounts for the observed lag and the biphasic nature of the time courses in Fig. 2 A is given by Eq. 4:

$$C* \xrightarrow{k_{np}} C \xrightarrow{k_t} I_1 \xrightarrow{k_t} I_2 \ldots \xrightarrow{k_t} I_{n-1} \xrightarrow{k_t} P \qquad (4)$$

In Eq. 4, C and C* are two conformations of the Hsp104-peptide complex in equilibrium. C* is the Hsp104-peptide complex that must first proceed through a step with rate constant k_{np} to form C, which represents Hsp104 bound to the peptide in a form that can proceed through ATP-driven translocation steps. The concentrations of these two species are accounted for by the fraction of productively bound complexes, x, and thus the fraction of nonproductively bound complexes would be given by $(1 - x)$. This step with rate constant k_{np} accounts for the biphasic character of the kinetic time courses. Next, to account for the lag in the kinetic time course, C can proceed through n number of steps with rate constant k_t before dissociation into P, see Methods (Eq. 3).

In the context of the mechanism proposed by Gates et al. (25), C* and C could represent two conformations of the ATPγS bound "closed" conformation observed by cryo-EM, with k_{np} representing the conformational change for that transition. Then, k_t may represent the ratcheting steps that advance the peptide by two amino acids through the axial channel of Hsp104 hexamers. Although the current assay does not allow the attribution of the observed kinetic phases to specific mechanical movements, the observations here do not conflict with the mechanistic model proposed by Gates et al. (25).

The time courses shown in Fig. 2 A (solid traces) were individually fit to the expression derived from Eq. 4 (see

Please cite this article in press as: DurieLin et al., Hsp104 and Potentiated Variants Can Operate as Distinct Nonprocessive Translocases, Biophysical Journal (2019), https://doi.org/10.1016/j.bpj.2019.03.035

Supporting Data). Best fit lines are shown as broken black traces in Fig. 2 A. The parameters from these fits are summarized in the first three rows of Table 2 (mean ± SE, three replicates). Note that these time courses were not well described by a simple sum of exponential equations due to the observed lag (fit not shown). The values for the parameters k_t, n, and x, where x is the fraction of starting complex in the C conformation, exhibited no discernable length-dependent trends and are summarized in the first three rows of Table 2.

The values of k_{np} were noted to vary such that faster rate constants are observed with shorter peptides. One possible explanation has to do with the binding location or environment. If 26 amino acids are inside the channel as reported by Gates et al., then there are fewer points of contact for the 30mer compared to the 50mer. If Hsp104 is more likely to bind at or near an end on the 30mer, and it more rapidly transitions from a nonproductive to a productive complex upon mixing with ATP, then it is possible that binding positions nearer the end of the peptide favor transitions to the productive complex compared to binding positions in the center of the peptide.

The average and standard error of the number of steps, n, from individual nonlinear least squares (NLLS) fits of the time courses in Fig. 2 A to Eq. 4 are shown in Fig. 2 B. The number of repeating steps n taken by Hsp104 is constant across the lengths of the substrate tested for Hsp104, with the average $n = (1.6 \pm 0.1)$ steps. As noted above, a lag results from the observation of more than one step with similar rate constants. For comparison, the number of steps taken by the processive translocase ClpA varied linearly from $n = 1.4$ steps to 3.0 steps in an identical experiment (12).

If these steps represent repetitions of a two amino acid translocation step, then the extent of the lag would be predicted to vary with substrate length for processive translocation (12,13,29,30,44–47). The formal possibility described in Fig. 1, G and H cannot be ruled out from this experiment; however, the simulations predict 13 steps when 26 amino acids are occluded, although we observe only two repeated steps. For the scenario illustrated in Fig. 1, G and H to give rise to these results, only the terminal four residues of the substrate would be bound in the Hsp104 hexamer, with the remainder of the peptide substrate extending from the NDB2 end of the Hsp104 hexamer. This possibility is not supported by structural work showing bound peptides extending from the NBD1 end of the Hsp104 hexamer (25).

Thus, we are left with one of two explanations. 1) Hsp104 exhibits low processivity (i.e., the disaggregase takes one or two steps before dissociation independent of length and binding position). 2) Translocation is very fast relative to the one to two steps we detect in this experiment.

A sufficiently long substrate will exhibit a length dependence even if translocation is fast relative to the two steps we detect using the relatively short RepA substrates. Thus, we next used longer substrates, namely fluorescein-labeled truncations of α-casein, which were 102 and 127 amino acids in length. α-casein has been used as a substrate previously to examine Hsp104 function (7,20,25). We have previously used these truncations of α-casein to examine the binding of both ClpA and ClpB. We showed that 127 amino acids and shorter would accommodate only one hexamer of either ClpA or ClpB, whereas longer constructs could accommodate two hexamers (39,48). We applied the same experimental design schematized in Fig. 1 B with the exception that anisotropy was detected instead of fluorescence. Fluorescence anisotropy was used because it reflects the resident time of the motor on the substrate regardless of directionality (see Methods). As observed with the 30–50 amino acid substrates, Fig. 2 C shows a lag in the Hsp104-catalyzed translocation and dissociation time course for both the 102 and 127 amino acid substrates, and the lengths of the lags are indistinguishable. In contrast to the observations with Hsp104, the processive translocase ClpA exhibits a length-dependent lag in the same experimental design (Fig. S5), as previously reported (23).

Anisotropy time courses are influenced by both anisotropy and fluorescence quantum yield. Consequently, the kinetic time courses require a simultaneous analysis of total fluorescence and anisotropy. We subjected the anisotropy time courses and their corresponding total fluorescence time courses to NLLS analysis using the strategy described by Otto et al. (49). The time courses for α-casein 102 and 127 were both well described by a model with two kinetic steps (see Fig. S4 and corresponding Supporting Data). This observation is consistent with Hsp104 taking one to two translocation steps even on substantially longer polypeptide substrates compared to the RepA peptides and is

TABLE 2 Kinetic Parameters Determined from Individual NLLS Fitting of Hsp104 Time Courses

Protein	Peptide Length (Amino Acids)	k_{np} (s^{-1})	x	k_t (s^{-1})	n (Steps)	Variance[a]
Hsp104	30	0.032 ± 0.001	0.67 ± 0.01	0.133 ± 0.007	1.51 ± 0.09	$1.95 \times 10^{-5} - 8.59 \times 10^{-5}$
Hsp104	40	0.010 ± 0.001	0.70 ± 0.04	0.106 ± 0.007	1.52 ± 0.08	$3.45 \times 10^{-6} - 7.04 \times 10^{-6}$
Hsp104	50	0.0069 ± 0.0002	0.61 ± 0.01	0.147 ± 0.007	1.88 ± 0.02	$2.89 \times 10^{-6} - 1.90 \times 10^{-5}$
$Hsp104^{A503S}$	30	0.0085 ± 0.0009	0.44 ± 0.04	0.11 ± 0.01	1.00 ± 0.04	$1.62 \times 10^{-5} - 2.28 \times 10^{-5}$
$Hsp104^{A503S}$	40	0.0053 ± 0.0002	0.36 ± 0.02	0.14 ± 0.02	1.22 ± 0.06	$2.02 \times 10^{-6} - 1.04 \times 10^{-5}$
$Hsp104^{A503S}$	50	0.0055 ± 0.0002	0.30 ± 0.02	0.13 ± 0.02	1.22 ± 0.06	$3.57 \times 10^{-6} - 7.23 \times 10^{-6}$

The uncertainties on the parameters represent the SE of three independent determinations.
[a]The variance column reports the range of values for the fits to Eq. 4 for three replicates.

Please cite this article in press as: DurieLin et al., Hsp104 and Potentiated Variants Can Operate as Distinct Nonprocessive Translocases, Biophysical Journal (2019), https://doi.org/10.1016/j.bpj.2019.03.035

not consistent with complete threading or highly processive translocation.

Directionality of Hsp104-driven polypeptide translocation

We tested whether Hsp104 displayed a directional bias in its translocation of peptide substrates. Though length dependence was not observed for N-labeled peptides (Fig. 2, A–C), we tested whether C-labeled peptides reveal length-dependent time courses. In a previous study using this experimental design, the position of the fluorophore relative to the ClpA-binding site yielded information on directionality (12). The RepA truncation peptides and the 127 amino acid casein truncation peptide were prepared with the label at the C-terminus (see Table 1) and tested using the same experimental designs. Again, a lag was observed in the time courses from the 30, 40, and 50 amino acid peptides, and again, the number of steps taken was independent of substrate length (Fig. S6 A; Table S2). Additionally, the anisotropy time courses of the N-labeled and C-labeled 127 amino acid casein substrates were indistinguishable (Fig. S6 B). If there is any directional bias of Hsp104-catalyzed polypeptide translocation, it is not detectable in this experimental design.

Polypeptide translocation mechanism of a potentiated Hsp104 variant

$Hsp104^{A503S}$ is a variant of Hsp104 engineered to provide enhanced disaggregation, specifically against aggregation-prone proteins implicated in neurodegenerative disease (7,50). Remarkably, in addition to promising results in many in vitro and yeast studies, this potentiated variant prevents neurodegeneration in a *C. elegans* model of Parkinson's disease (7). Moreover, $Hsp104^{A503S}$ rescues FUS aggregation in mammalian cells (8). Could a difference in processivity relative to WT Hsp104 be the basis for the therapeutic gain of function exhibited by $Hsp104^{A503S}$? To test this possibility, we repeated the experiments schematized in Fig. 1 B with the $Hsp104^{A503S}$ variant in place of $Hsp104^{WT}$.

Fig. 2 D (solid traces) displays representative time courses from the $Hsp104^{A503S}$-peptide complex prepared with $RepA_{Flu1–30}$, $RepA_{Flu1–40}$, and $RepA_{Flu1–50}$. Comparing the time courses from Hsp104 and $Hsp104^{A503S}$, two differences are observed. First, the $Hsp104^{A503S}$ time courses needed to be longer to capture the full reaction (compare insets in Fig. 2, A and D). $Hsp104^{A503S}$ is in contact longer with the peptide compared to Hsp104. Second, in contrast to the time courses in Fig. 2 A for $Hsp104^{WT}$, a lag is not obvious in the $Hsp104^{A503S}$ time courses (Fig. 2 D). Nonetheless, the $Hsp104^{A503S}$ time courses were fit in the same manner as those from the WT protein to test for the presence of a lag not detected by visual inspection and to make direct comparisons of the parameters between the time courses generated by Hsp104 and $Hsp104^{A503S}$. The time courses were individually fit to the equation derived from Eq. 4 as described in Methods. Best fit lines are shown as broken black traces in Fig. 2 D, and parameters are summarized in the last three rows of Table 2 (means ± SE, three replicates).

Consistent with our qualitative assessment, the quantitative analysis does not reveal a lag at any length of peptide tested (Fig. 2 D). Across the three lengths tested, $n = (1.1 \pm 0.1)$ steps (Fig. 2 E). Thus, at saturating ATP, the number of repeating steps is within the error of unity. No additional repeats of the step with rate constant k_t were observed regardless of the length of the polypeptide substrate. These findings suggest that $Hsp104^{A503S}$ therapeutic gain of function is not due to increased processivity against soluble polypeptides.

Proposal of a minimal model for Hsp104-catalyzed polypeptide translocation

The time courses presented in Fig. 2 were collected in saturating ATP conditions (5 mM reaction concentration). Under these conditions, we observed that the kinetic step k_t was repeated one to two times with $\langle n \rangle = (1.6 \pm 0.1)$ steps. If those steps represent translocation, then the observed repeating step would be coupled to ATP binding. This hypothesis predicts that the observed rate constant would depend on [ATP]. To test this possibility, we performed the experiments schematized in Fig. 1 B with varied concentrations of ATP in the second syringe.

Fig. 3, A and B shows a representative set of time courses from the Hsp104-catalyzed translocation of $RepA_{Flu1–50}$ with ATP concentrations ranging from 10 μM ATP (red trace) through 5 mM ATP (purple trace). Residuals from the fits of these time courses are shown in the Supporting Data (see Fig. S7). The time courses are dependent upon ATP concentration, consistent with the idea that the signal is sensitive to ATP-driven steps that must occur before Hsp104 dissociates from the polypeptide. Inspection of the time courses reveals that the curves shift to the right, or are slower, with decreased ATP concentrations.

Consistent with our observations in the presence of saturating ATP (Fig. 2 A), the time courses in Fig. 3 A exhibit biphasic character across the full range of ATP concentrations tested. Likewise, a lag is observed in the time courses shown in Fig. 3 A.

We sought to understand the functional dependence on ATP to describe the mechanism by which Hsp104 translocates polypeptide substrate. We demonstrated that the time courses collected as a function of substrate length (Fig. 2 A) could be described by Eq. 4, written generally for n steps. From the analysis of those fits, we observed that n is between one and two steps. Eq. 5 represents a reduction of Eq. 4, and in addition to k_{np}, which was described in the context of Eq. 4, includes two observed rate constants,

Please cite this article in press as: DurieLin et al., Hsp104 and Potentiated Variants Can Operate as Distinct Nonprocessive Translocases, Biophysical Journal (2019), https://doi.org/10.1016/j.bpj.2019.03.035

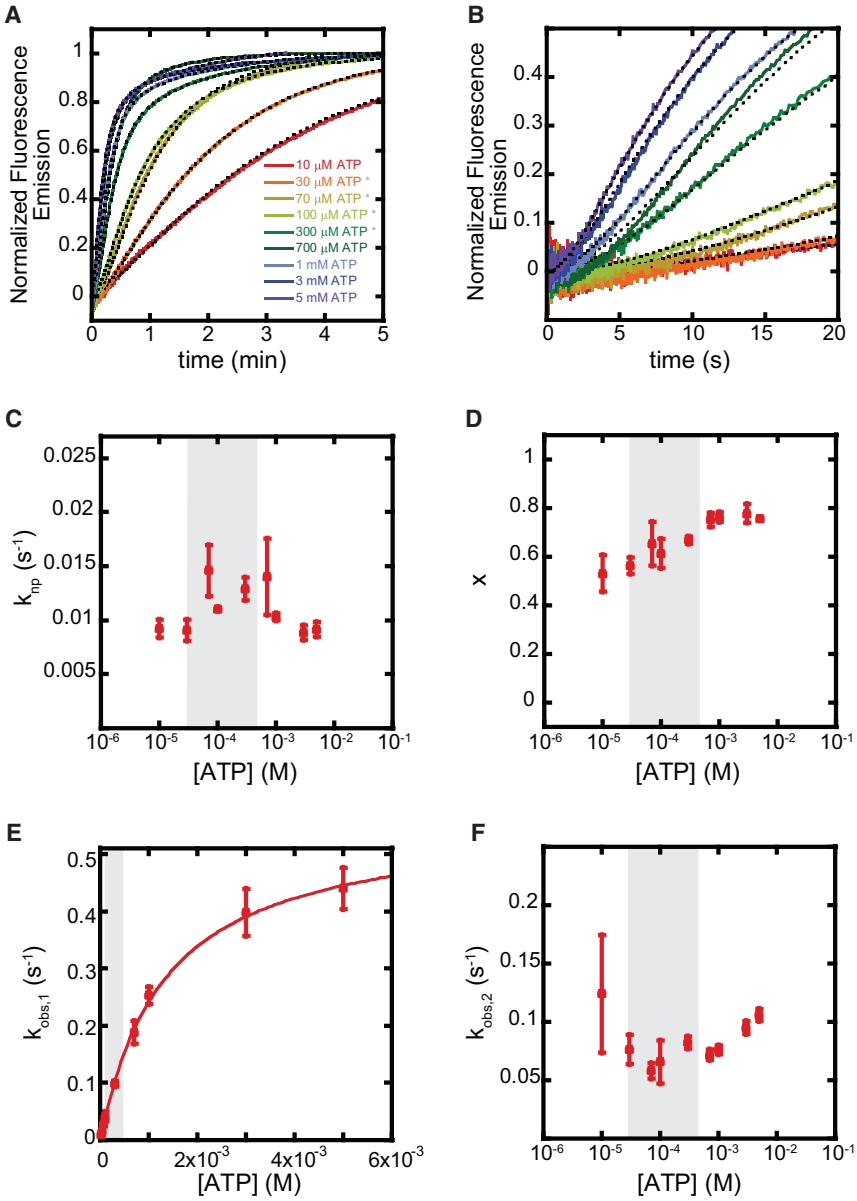

FIGURE 3 ATP dependence of Hsp104 catalyzed the polypeptide translocation. Representative ATP-dependent Hsp104-catalyzed polypeptide translocation time courses are presented to show the overall shape of the curve throughout the length of the time course (*A*) as well as the early part of the time course in which the lag is present (*B*). The experimental data are shown as solid colored traces. Each color corresponds to a different ATP concentration, with 10 μM ATP shown in red. Intermediate concentrations of ATP go through orange, green, and blue, with the highest concentration, 5 mM ATP, shown in purple. The ATP concentrations that fall within the range of ATP:ATPγS that enhance Hsp104 activity are denoted by a gray asterisk. The broken black traces represent the best fit lines of each time course, individually, to the equation derived from Eq. 5 using NLLS analysis. (*C–F*) Shown are secondary plots of the parameters from individual fits of time courses to Eq. 5 as a function of [ATP]. Parameters are (*C*) k_{np}, (*D*) x (the fraction of complex in the C or productive conformation), (*E*) $k_{obs,1}$, and (*F*) $k_{obs,2}$. (mean $\pm$ SE, n = 3). In (*E*), the curve represents the best fit of the data to a rectangular hyperbola, Eq. 6. The shaded region of the plot represents the range of ATP concentrations, which correspond to the ATP:ATPγS ratios that elicit enhanced Hsp104 activity. To see this figure in color, go online.

$k_{obs,1}$ and $k_{obs,2}$. Descriptions of the other variables are as defined for Eq. 4.

$$C* \xrightarrow{k_{np}} C \xrightarrow{k_{obs,1}} I \xrightarrow{k_{obs,2}} P \tag{5}$$

Each time course shown in Fig. 3, A and B was individually fit to Eq. 5 as described in Methods, with the fits shown in black broken lines. Parameters are displayed in Fig. 3, C–F (mean $\pm$ SE, three replicates). It is important to note that the equation describing these time courses is symmetric. There is no information in the name of the parameter about the order in which each kinetic step occurs. The kinetic step with the rate constant reported as $k_{obs,1}$ may occur before or after the kinetic step with rate constant $k_{obs,2}$ and vice versa.

From the secondary plot in Fig. 3 C, k_{np} appears to be independent of ATP concentration with k_{np} = (0.011 $\pm$ 0.002) s^{-1}. The fraction of the starting complex that begins in the productive complex, x, varies across the range of [ATP] tested from a low of 0.53 $\pm$ 0.07 to a high of 0.78 $\pm$ 0.04 (Fig. 3 D). The higher x values are observed at higher [ATP], but many of the individual measurements are within the error of each other such that a clear trend is not defined.

There is a clear dependence of $k_{obs,1}$ on ATP concentration (Fig. 3 E). This dependence is well described by a rectangular hyperbola given by

$$k_{obs,x} = \frac{k_{obs,x,max,}[ATP]}{K_{1/2} + [ATP]}. \tag{6}$$

From fitting the data in Fig. 3 E to Eq. 6, we find $k_{obs,1,max}$ = (0.56 $\pm$ 0.01) s^{-1} and $K_{1/2}$ = (1.3 $\pm$ 0.1) mM (errors reported from the fit to Eq. 6). A kinetic step that is in rapid

Please cite this article in press as: DurieLin et al., Hsp104 and Potentiated Variants Can Operate as Distinct Nonprocessive Translocases, Biophysical Journal (2019), https://doi.org/10.1016/j.bpj.2019.03.035

equilibrium with ATP binding gives rise to a hyperbolic dependence on [ATP] as observed in Fig. 3 E, indicating that $k_{obs,1}$ is kinetically coupled to ATP binding. This indicates that at least one observed step is coupled to ATP binding and therefore represents an ATP-driven step. We also note that this reported maximal rate constant is similar to previously reported Hsp104 ATPase rates from steady-state experiments of 0.2–0.8 s^{-1}, although there are differences in the experimental conditions in this study and these previous reports (34,51,52). In contrast, the rate constant $k_{obs,2}$ appears to be independent of ATP concentration across the range of ATP concentrations tested (Fig. 3 F). All of the points are within one SE of the mean, $k_{obs,2} = (0.08 \pm 0.02)$ s^{-1}.

Earlier work has shown that ratios of ATP:ATPγS between 3:1 to 1:5 elicit enhanced disaggregase activity in the absence of Hsp70 (40,53,54). We did not observe such an effect in our experiments (see Fig. S8). The experiments that fall within this range of ATP:ATPγS ratios include the 30–300 μM ATP conditions, shown in the orange through green traces and marked with an asterisk in the in-plot legend in Fig. 3, A and B. The region of the secondary plots that fall within this condition is also shaded in gray in Fig. 3, C–F. One important difference between the experimental design used here compared to the activity assays used previously (40,53,54) is that our assay monitors a single turnover of the Hsp104-peptide complex. In contrast, prior experiments are performed over longer time frames and allow for multiple rounds of Hsp104 engagement with polypeptide substrate. In addition, our assay uses a relatively short, model unfolded peptide. This substrate is appropriate for a study of the molecular mechanism of polypeptide translocation. The substrates used previously include RepA dimers, aggregated green fluorescent protein (GFP), and $RepA_{1-70}$GFP in which the GFP portion is folded and fluorescent. Using differing experimental designs provides insight into different aspects of the mechanism.

$Hsp104^{A503S}$ translocation exhibits altered ATP coupling

The A503S mutation is located in the middle domain of Hsp104, a region implicated in the modulation of Hsp104 ATPase activity (3). We tested whether the A503S mutation changes the way in which Hsp104 couples ATP binding and hydrolysis to polypeptide translocation. Thus, ATP concentration-dependence experiments described for $Hsp104^{WT}$ in Fig. 3 were repeated with $Hsp104^{A503S}$.

Fig. 4, A and B show a representative set of time courses from the $Hsp104^{A503S}$ catalyzed translocation of $RepA_{Flu1-50}$ with ATP concentrations ranging from 10 μM ATP through 5 mM ATP. The time courses shown in Fig. 4, A and B are noted to be slower or shifted to the right as the ATP concentration is reduced. Again, this observation is consistent with the idea that the kinetic steps we detect in this assay are coupled to ATP binding, and because the signal comes from the peptide, these steps must occur before Hsp104 dissociates. At each [ATP] tested, the time course from $Hsp104^{A503S}$ (Fig. 4, A and B) is slower than the corresponding [ATP] time course from Hsp104 (Fig. 3, A and B). Another potentiated variant that exhibits similar activity to $Hsp104^{A503S}$, $Hsp104^{A503V}$ (7), displays increased disaggregase activity at ratios of ATP:ATPγS of 1:0 to 1:0.667 in the absence of Hsp70 (54). This range of ATP:ATPγS includes the 100 μM ATP and higher ATP concentrations shown as the light green through purple traces and marked with an asterisk in the in-plot legend in Fig. 4, A and B.

Unlike Hsp104, no lag was observed in the data collected at saturating ATP for $Hsp104^{A503S}$ (Fig. 2 D). Here, we observe no lag across the range of [ATP] tested. Furthermore, $Hsp104^{A503S}$ time courses were as well described by a sum of two exponentials as by the equation derived from Eq. 4 with n = 1. When the $Hsp104^{A503S}$ time courses at saturating ATP (Fig. 2 D) were fit to the sum of two exponentials, one observed rate constant had the same value as the best fit parameter k_{np} from Eq. 4 and the other observed rate constant had the same value as the best fit parameter k_t from Eq. 4. The time courses generated by $Hsp104^{A503S}$ do not exhibit a third kinetic step as observed for $Hsp104^{WT}$. Thus, these time courses are well described by a further simplification of Eq. 4, shown as Eq. 7 below.

$$C^* \xrightarrow{k_{np}} C \xrightarrow{k_{obs,1}} P \tag{7}$$

In other words, one rate constant observed for the $Hsp104^{WT}$ time courses is not observed in the $Hsp104^{A503S}$ time courses. Two possibilities could explain this difference. One is that the kinetic mechanism is completely different for the $Hsp104^{WT}$ versus $Hsp104^{A503S}$ and so the kinetic steps observed for $Hsp104^{A503S}$ are not those observed for $Hsp104^{WT}$ translocation. The other possibility is that the point mutation (A503S) affected one or more of the steps observed in the WT mechanism, for example, slowing a rate constant and/or affecting coupling to ATP.

Thus, for fitting the time courses shown in Fig. 4, we used an equation derived from Eq. 7. The low [ATP] time courses (10, 30, and 70 μM ATP) were well described by a single kinetic phase, consistent with the rate constant k_{np} (54). The best fit lines are shown as broken black traces in Fig. 4, A and B. Rate constants are shown in Fig. 4, C and E (means ± SE, three replicates).

Consider the observed rate constant $k_{np,A503S}$ (Fig. 4 C, red circles). This rate constant $k_{np,A503S} = (0.0056 \pm 0.0007)$ s^{-1} is independent of ATP concentration and is the slower of the two observed rate constants. In our examination of $Hsp104^{WT}$ time courses, $k_{np,WT}$ was independent of [ATP] and was the slowest observed rate constant at $k_{np,WT} = (0.011 \pm 0.002)$ s^{-1}. If the rate constant $k_{np,A503S}$ reflects the same step as $k_{np,WT}$ (Fig. 4 C, black squares), then this kinetic step is twice as fast for $Hsp104^{WT}$ as for

Please cite this article in press as: DurieLin et al., Hsp104 and Potentiated Variants Can Operate as Distinct Nonprocessive Translocases, Biophysical Journal (2019), https://doi.org/10.1016/j.bpj.2019.03.035

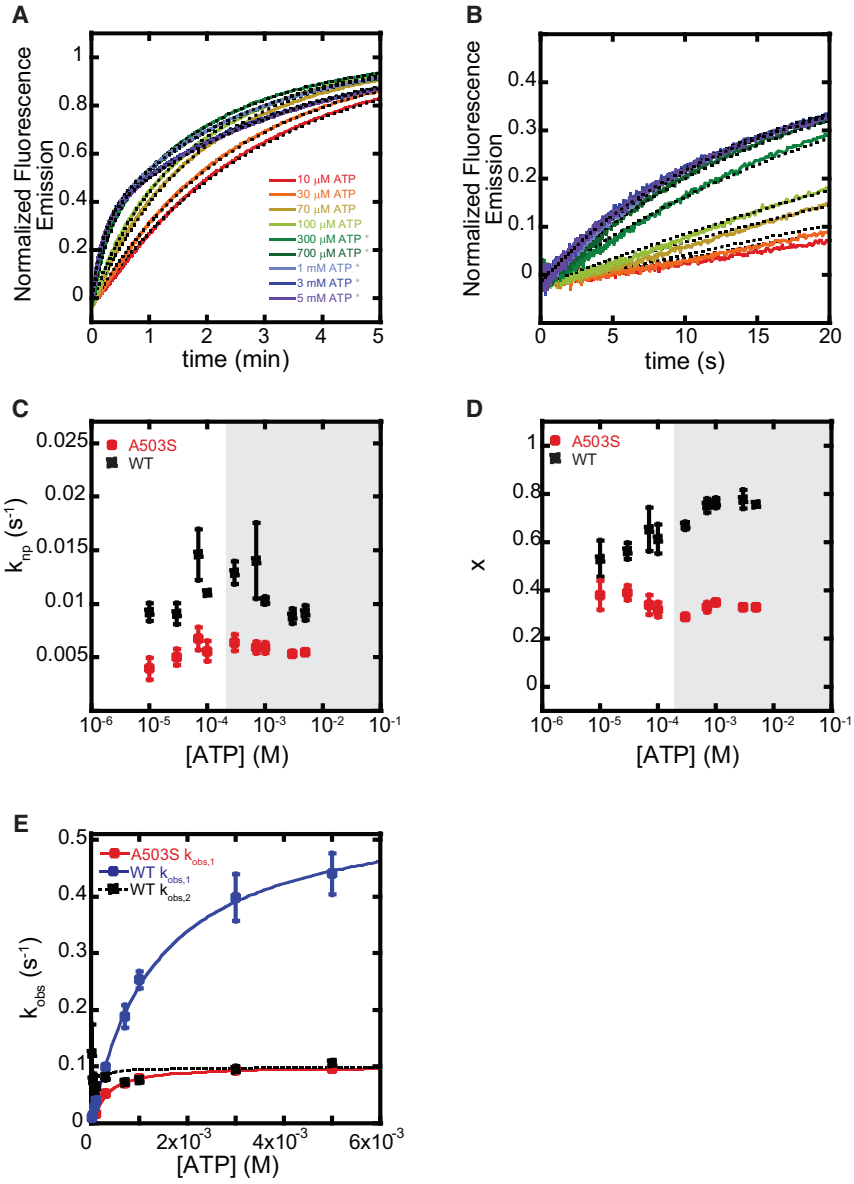

FIGURE 4 ATP dependence of Hsp104^{A503S} catalyzed polypeptide translocation. (*A* and *B*) Representative ATP-dependent time courses are shown. The experimental data are shown as solid colored traces. Each color corresponds to a different ATP concentration, with 10 μM ATP shown in red following the same color pattern as in Fig. 3. The ATP concentrations that fall within the range of ATP:ATPγS that enhances Hsp104^{A503V} activity are denoted by a gray asterisk. Two timescales are presented to show the overall shape of the curve throughout the length of the time course (*A*) as well as the early part of the time course in which the lag is present at high ATP for the WT protein but not for the variant (*B*). The broken black traces represent the best fit lines of each time course, individually, to a single exponential for 10, 30, and 70 μM ATP and to Eq. 7 for the remaining [ATP]. (*C–E*) Shown are the secondary plots of the parameters from those individual fits as a function of [ATP] (means ± SE, three replicates) with Hsp104^{A503S} translocation parameters shown in red circles. In (*C*), $k_{np,WT}$ is overlaid for comparison in black squares. The shaded region of the plot represents the range of ATP concentrations that correspond to the ATP:ATPγS ratios that elicit enhanced Hsp104^{A503V} activity. In (*D*), *x*, the fraction of complex in the *C* or productive conformation, from WT is again overlaid in black squares. In (*E*), the red circles are from the fits of the Hsp104^{A503S} time courses with 100 μM ATP – 5 mM ATP. The red curve represents the best fit of the data to a rectangular hyperbola with $k_{obs,1,A503S,max}$ = (0.1000 ± 0.0002) s^{-1}, and $K_{1/2,A503S}$ = (160 ± 40) μM. Errors reported are from the fit of the data displayed in (*E*) to Eq. 6. In (*E*), rate constants from fits of the translocation time courses catalyzed by Hsp104 are overlaid in blue circles ($k_{obs,1,WT}$) and black squares ($k_{obs,2,WT}$). To see this figure in color, go online.

Hsp104^{A503S}. Note that the value of *x*, the fraction of Hsp104-peptide complex in the productive form *C*, remains relatively flat at ~0.4 across all ATP concentrations tested for Hsp104A^{503S}, whereas the value of *x* for WT increases slightly with increasing ATP (Fig. 4 D). This suggests that A503S binds ATPγS more tightly than does WT. For WT, higher ratios of ATPγS:ATP result in similarly low values of *x* (Table S3, second row). The observation that the A503S mutation alters nucleotide binding and hydrolysis is consistent with the mutation's location within the regulatory M domain.

Finally, we observe a clear dependence of $k_{obs,1,A503S}$ on ATP concentration, Fig. 4 E (red circles). These data were well described by a rectangular hyperbola (Fig. 4 E, red line, Eq. 6). From fitting the data in Fig. 4 E to Eq. 6, we find that $K_{1/2,A503S}$ = (160 ± 40) μM, and $k_{obs,1\ max,A503S}$ = (0.100 ± 0.005) s^{-1} (errors reported from the fit to Eq. 6). This rate constant could reflect the same kinetic step observed for the WT protein as either $k_{obs,1,WT}$ (Fig. 4 E, blue circles) or $k_{obs,2,WT}$ (Fig. 4 E, black squares).

If we compare the ATP-dependent rate constant $k_{obs,1,A503S}$ (Fig. 4 E, red circles) with the ATP-dependent rate constant $k_{obs,1,WT}$ (Fig. 4 E, blue circles), we note that the maximal rate constant is fivefold lower for A503S compared to WT and that ATP affinity is an order of magnitude tighter for A503S than for WT. Alternatively, if we compare the ATP-dependent rate constant $k_{obs,1,A503S}$ (Fig. 4 E, red circles) with the ATP-independent rate constant for Hsp104^{WT} ($k_{obs,2,WT}$, Fig. 4 E, black squares), we note that the maximal rate for A503S is indistinguishable from the rate observed for WT. This finding would indicate that the apparent ATP-independence of $k_{obs,2}$ for Hsp104^{WT}

Please cite this article in press as: DurieLin et al., Hsp104 and Potentiated Variants Can Operate as Distinct Nonprocessive Translocases, Biophysical Journal (2019), https://doi.org/10.1016/j.bpj.2019.03.035

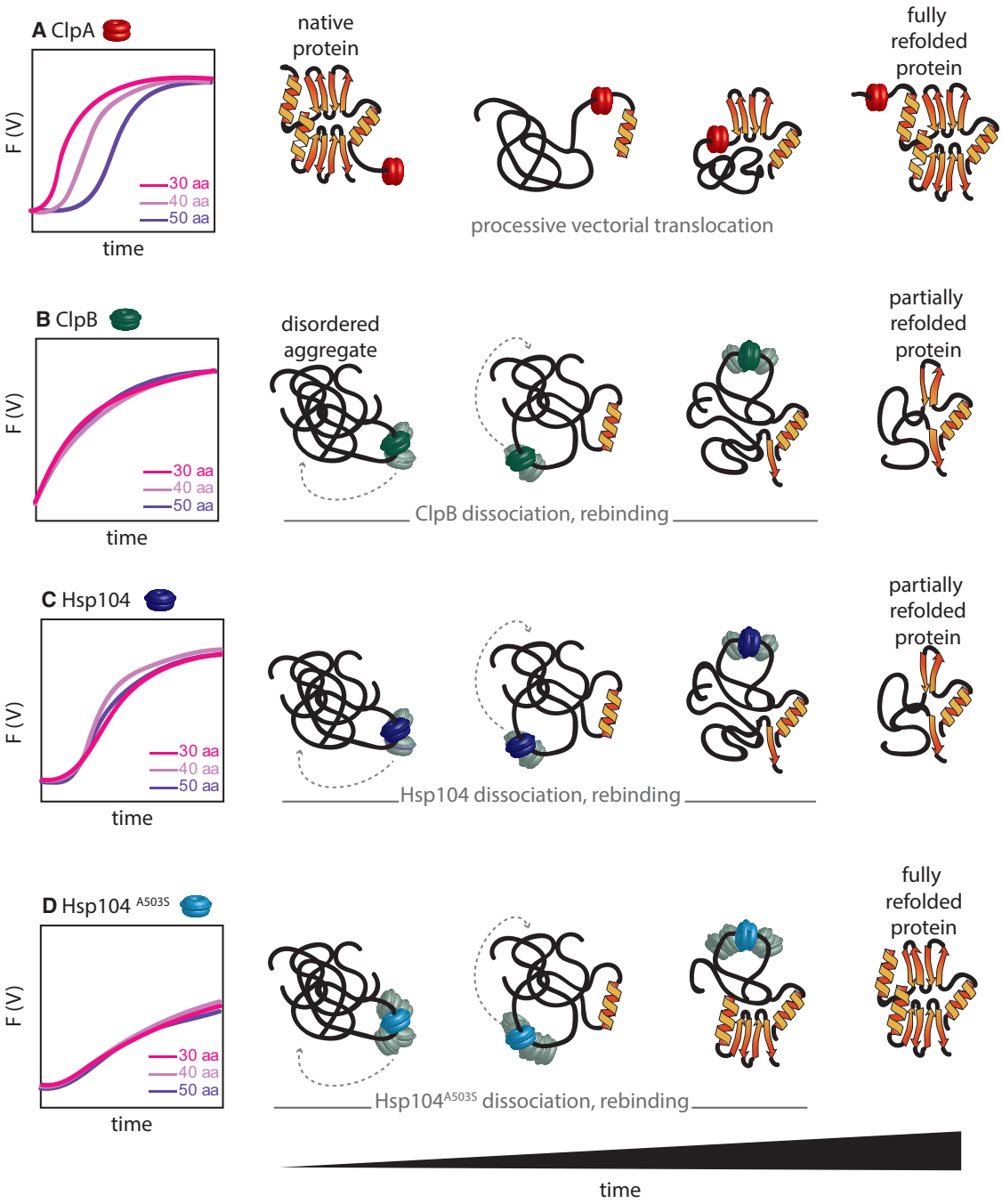

FIGURE 5 Comparison of ClpA, ClpB, Hsp104, and Hsp104^{A503S} transient state kinetics and mechanisms. In (*A*), representative time courses are shown for ClpA (*red rings*) in the experimental design used in Fig. 1 B with 30, 40, and 50 amino acid soluble substrates. There is a clear length-dependent lag. This length-dependent lag is consistent with ClpA's known function as a processive, vectorial translocase. A pictoral representation of ClpA's interaction with a folded substrate over time is shown to the right of the time courses. ClpA first engages with an end of a protein substrate. Through many rounds of ATP binding and hydrolysis, ClpA translocates along the protein, unfolding the protein in the process. The protein can then refold to its native structure. In (*B*), representative time courses are shown for ClpB (*green*) in the same experimental design. Here, no lag is observed, and no length dependence is observed. Two ATP-dependent kinetic steps were observed with different rate constants. Thus, ClpB takes one or two kinetic steps that are coupled to ATP binding before dissociating from the substrate. These kinetic steps may include, for example, physical translocation of the substrate and/or conformational changes of the ClpB hexamer while bound to the substrate. In the pictoral representation of the mechanism, ClpB first binds a disordered aggregate. The gray rings represent the possible spaces ClpB may occupy while bound to the substrate, taking one or two kinetic steps before dissociation. ClpB's movement maximizes entropy in the system and, in the process, can loosen or stretch the part of the aggregate to which ClpB is bound. Then, upon dissociation, ClpB can bind another exposed area of the aggregate and repeat the process of entropic pulling, dissociation, and rebinding. This may allow portions of the aggregate to refold correctly. With the addition of the Hsp70 system, dysregulating mutations or certain ratios of ATP:ATPγS, the aggregate can be fully rescued by ClpB. (*C*) The representative time courses for Hsp104 (*dark blue*) in the same experimental design is shown. A lag is observed, but there is no length dependence.

(legend continued on next page)

Please cite this article in press as: DurieLin et al., Hsp104 and Potentiated Variants Can Operate as Distinct Nonprocessive Translocases, Biophysical Journal (2019), https://doi.org/10.1016/j.bpj.2019.03.035

may be the plateau of a rectangular hyperbola reflecting tight ATP-binding affinity. A rectangular hyperbola with a midpoint at 50 μM ATP is shown in a black broken trace in Fig. 4 E as an example of how a high affinity isotherm for $k_{obs,2,WT}$ as a function of [ATP] may look. In other words, the $K_{1/2}$ of $k_{obs,2,WT}$ for Hsp104^{WT} (Fig. 3 F) may be tighter than we can observe with this range of ATP concentrations. In that case, the A503S mutation has weakened the ATP affinity of this step compared to WT. Whether $k_{obs,1,A503S}$ represents the same kinetic step observed as $k_{obs,1,WT}$ or $k_{obs,2,WT}$, this observation suggests that the A503S mutation impacts the coupling of ATP binding to the observed rate constant. The third possibility, that the step reflected in $k_{obs,1,A503S}$ is a step not observed for the Hsp104^{WT}, cannot be ruled out until the identity of these steps is determined.

DISCUSSION

Engineered interactions between Hsp104 variants and the protease ClpP led to a prevailing model of a highly processive translocation of polypeptide, or complete threading, by Hsp104 (20). Indeed, HAP-ClpP effectively degrades amyloid fibrils (21). However, that method is potentially influenced by ATP-independent degradation and cannot be used to indicate processive translocation as we have shown for ClpB. Nevertheless, recent high-resolution structural studies were interpreted to indicate a repeated two amino acid step size coupled to ATP binding and hydrolysis (25). Here, we sought to test the structural model using transient state kinetic techniques and soluble polypeptides that do not require non-native interactions with a protease.

Here, we report evidence of Hsp104 taking, at most, two ATP-driven kinetic steps before dissociating from the polypeptide substrate. Based on static cryo-EM structures, Gates et al. recently proposed a physical translocation step size of two amino acids per step (25). If Hsp104 processively translocates a polypeptide chain using repeated steps with a step size of two amino acids, based on the potential binding sites illustrated in Fig. 1, we would anticipate a minimum of 13 ATP-driven steps before Hsp104 dissociates from the short polypeptides used here. Further, we would anticipate substantially more steps on the 102 and 127 amino acid α-casein substrates. The single turnover experiments performed here are sensitive to the slowest steps that must occur before dissociation from the polypeptide substrate. However, if the two observed kinetic steps do represent mechanical movement and the step size is two amino acids per step then, this would indicate that Hsp104 translocates only four amino acids before dissociation. Using Eq. 3 with m = 2 amino acids and N = 4 amino acids, then the processivity Pr = 0.61. This finding suggests that, like ClpB (23), Hsp104 may use a "tug and release" mechanism to resolve protein aggregates (Fig. 5). It is important to note that the tug and release mechanism that we have proposed would be mechanistically identical to the entropic pulling mechanism proposed by De Los Rios et al. (55).

The Cryo-EM results reported by Gates et al. clearly indicate that there are extended and closed conformations bound to α-casein (25). Assuming that the process of vitrification does not perturb the equilibrium, then the observed distribution of states represent the distribution of states present in the sample at thermodynamic equilibrium before vitrification. As with all thermodynamic measurements, there is no information on the path. With that in mind, there is no information in the electron micrographs on the path by which the extended and closed conformations arrived at the extended and closed conformations. Although the extended and closed conformations have been interpreted to represent translocation intermediates, the path information is not present within the observations. Consequently, it remains unknown if the closed conformation extends or if the extended conformation closes. An alternative explanation is that the extended and closed conformations could represent different binding modes on the α-casein substrate used in those experiments. For example, the extended and closed conformations could be the consequence of the α-casein binding N-terminally versus C-terminally. Regardless of the interpretation, there is no experimental evidence reported that indicates the extended and closed conformations represent translocation intermediates.

There are notable differences between the kinetic time courses collected for ClpB versus Hsp104. In particular, the same experimental design used with ClpB did not result in the observation of lag kinetics (23). The lag indicates that there is more than one kinetic step with similar rate constants. Thus, for Hsp104, the lag indicates that the kinetic steps we detect have a similar rate constant, whereas the two steps we detect for ClpB exhibit rate constants that are approximately an order of magnitude different (23). Regardless of these differences, for both ClpB and Hsp104 the two steps we detect are coupled to ATP binding, and they must happen before the enzyme dissociates from

Hsp104 also takes one or two kinetic steps, coupled to ATP binding, before dissociating from the substrate. The rate constants for these steps are similar, giving rise to the lag. The mechanistic interpretation for Hsp104 is the same as that for ClpB. Hsp104 binds a disordered aggregate, tugs on loose loops or ends via entropic pulling (possible space sampled shown by *gray rings*), dissociates, and can then rebind elsewhere on the aggregate to repeat this process. Also like ClpB, Hsp104 alone cannot fully rescue disordered aggregates. (*D*) The representative time courses for Hsp104^{A503S} (*light blue*) are shown. They are similar to those observed for Hsp104 in that there is a lag and there is no length dependence. The time courses are slower compared to Hsp104, however, indicating a longer time during which Hsp104^{A503S} is bound to the substrate. The pictorial display of the mechanism indicates that this allows for a greater range of sampled spaces or more entropic pulling. Although the basic process is the same (bind aggregate, loosen aggregate by entropic pulling, dissociate, and rebind), the longer residence time of Hsp104^{A503S} on the aggregate allows it to more effectively loosen the aggregate, such that this potentiated variant is able to fully rescue the aggregated proteins without the Hsp70 system or mixtures of ATP and ATPγS. To see this figure in color, go online.

Please cite this article in press as: DurieLin et al., Hsp104 and Potentiated Variants Can Operate as Distinct Nonprocessive Translocases, Biophysical Journal (2019), https://doi.org/10.1016/j.bpj.2019.03.035

the polypeptide chain. Thus, the detected kinetic steps are consistent with ATP-driven steps.

The observation that the kinetic steps detected here are coupled to ATP binding implies that we should detect the same step in an ATPase experiment. However, to fully understand the coupling of ATP binding and hydrolysis with peptide substrate translocation, there is an urgent need for a focused investigation of the dynamic distribution of oligomeric states of Hsp104, nucleotide-linked assembly, and the coupling of ATP hydrolysis to the various oligomeric states observed in solution (38). Without this context, individual ATPase measurements have limited applicability. We show in this work that ATP binding is coupled to the observed kinetic steps preceding the dissociation of hexameric Hsp104 from the polypeptide chain. But many additional futile sources of ATP hydrolysis remain possible. For example, Hsp104 contains two ATP binding and hydrolysis sites per monomer and therefore 12 ATP sites per hexameric ring. Thus, there are significantly more ATPase sites than may be involved in the energy-driven steps in a hexamer bound to a peptide substrate. There are even more sources of ATP hydrolysis possible if lower order oligomers hydrolyze ATP, which is currently unknown. A series of studies are underway to characterize the self-association of Hsp104 hexamers, the nucleotide-linked oligomerization of Hsp104, and the ATPase activity of Hsp104 in a dynamic equilibrium of oligomeric states.

The substrate itself may impact the translocation mechanism of Hsp104. For example, a more structured substrate, such as folded GFP or an amyloid aggregate, may exploit the plasticity of the Hsp104 mechanism (53) and elicit additional translocation steps. Additionally, collaborating chaperones, such as Hsp70 and Hsp40, may affect the mechanism of Hsp104. Hsp104 can dissolve amyloid independently from the Hsp70 system (53,56,57), but Hsp104 disaggregase activity against amyloid and disordered aggregates can be greatly stimulated by the Hsp70 system (2,53,58). Conditions have been found and widely used in vitro to examine peptide binding, substrate-activated ATP hydrolysis, and the threading, unfolding, or disaggregation of protein substrates by Hsp104 in the absence of the Hsp70 system (7,20,34,40,59–61). Our recent work with *E. coli* ClpB and DnaK, the bacterial homologs of Hsp104 and Hsp70, respectively, revealed that DnaK at sufficiently high concentrations to saturate the binding to ClpB triggers a release of peptide substrate from ClpB (62). Thus, under normal cellular conditions, DnaK binding to ClpB may sequester ClpB in a low peptide affinity state, and upon cellular stress, DnaK dissociates from ClpB to bind denatured clients, thereby unleashing ClpB in a high peptide affinity state to disentangle aggregates through a tug and release mechanism (62).

$Hsp104^{A503S}$ was developed to target substrates associated with neurodegenerative disease. This potentiated variant has been shown to suppress toxicity, solubilize aggregates, and restore proper cellular location in yeast and mammalian studies (7,41,50). $Hsp104^{A503S}$ has also been shown to protect neurons from degeneration in a *C. elegans* model of Parkinson's disease (7). We considered whether this variant may gain its increased disaggregation activity by enhanced processivity. Subjecting the potentiated variant $Hsp104^{A503S}$ to the same experimental designs revealed that $Hsp104^{A503S}$ takes even fewer kinetic steps than Hsp104.

The location, A503, of the single missense mutation that imparts these enhanced activities suggests a regulatory effect. This position is in helix L3 of the middle domain of Hsp104. The middle domain regulates communication between NBD1 and NBD2 and also serves as the site of Hsp70 binding (63–67). How does a single missense mutation in this position enhance Hsp104 disaggregase activity? Although this remains an open question, our observations suggest that one effect of the mutation is to alter the coupling of ATP hydrolysis to translocation.

The unleashed disaggregase activity of $Hsp104^{A503S}$ corresponds to a slower dissociation from the peptide substrate compared to the unmodified protein (compare Fig. 3, A and B with Fig. 4, A and B). This observation is consistent with other reports in the field. A mixture of ATP with the slowly hydrolyzable analog ATPγS can increase Hsp104 activities, including substrate unfolding, disaggregation, and reactivation (40). The bacterial homolog ClpB was shown to have an increased unfolding capability when the WT protein was "doped" with hydrolysis-deficient mutants (68). Taken together, these findings suggest that modulating ATP hydrolysis in such a way as to extend the amount of time during which Hsp104 is engaged with the peptide substrate may be the key in regulating Hsp104 activity. Analogous to how one might untangle a strand of lights or a delicate necklace, the disaggregating motors may exert some mechanical force on exposed loops or the ends of an aggregate, possibly even moving back and forth rather than in a constant direction. This concept is similar to "entropic pulling" proposed by Goloubinoff to explain the mechanisms of Hsp70s (55). Essentially, the bound disaggregase prefers greater freedom of movement, which is achieved by gaining distance from the surface of an aggregate. The conditions that slow dissociation from the peptide substrate or increase the residence time of the motor on the substrate protein are shown to be more effective for Hsp104-catalyzed disaggregation.

SUPPORTING MATERIAL

Supporting Material can be found online at https://doi.org/10.1016/j.bpj.2019.03.035.

AUTHOR CONTRIBUTIONS

C.L.D. and A.L.L. designed experiments. C.L.D. performed experiments and analyzed the data. N.W.S. performed selected anisotropy experiments.

Please cite this article in press as: DurieLin et al., Hsp104 and Potentiated Variants Can Operate as Distinct Nonprocessive Translocases, Biophysical Journal (2019), https://doi.org/10.1016/j.bpj.2019.03.035

N.W.S. and A.L.L. analyzed anisotropy data. M.J., J.L., K.L.M., E.A.S., and L.M.C. expressed and purified proteins. C.L.D. and A.L.L. wrote the manuscript with contributions from J.L., N.W.S., K.L.M., M.E.J., and J.S. All authors read and approved the final manuscript.

ACKNOWLEDGMENTS

We thank Amber Tariq for assistance with Hsp104 preparations.

This work was supported by the National Science Foundation (grant MCB-1412624 to A.L.L.) and the National Institutes of Health (grant R01GM099836 to J.S.).

REFERENCES

1. Parsell, D. A., A. S. Kowal, …, S. Lindquist. 1994. Protein disaggregation mediated by heat-shock protein Hsp104. *Nature.* 372:475–478.
2. Glover, J. R., and S. Lindquist. 1998. Hsp104, Hsp70, and Hsp40: a novel chaperone system that rescues previously aggregated proteins. *Cell.* 94:73–82.
3. Sweeny, E. A., and J. Shorter. 2016. Mechanistic and structural insights into the prion-disaggregase activity of Hsp104. *J. Mol. Biol.* 428:1870–1885.
4. Schirmer, E. C., J. R. Glover, …, S. Lindquist. 1996. HSP100/Clp proteins: a common mechanism explains diverse functions. *Trends Biochem. Sci.* 21:289–296.
5. Erives, A. J., and J. S. Fassler. 2015. Metabolic and chaperone gene loss marks the origin of animals: evidence for Hsp104 and Hsp78 chaperones sharing mitochondrial enzymes as clients. *PLoS One.* 10:e0117192.
6. Jackrel, M. E., and J. Shorter. 2015. Engineering enhanced protein disaggregases for neurodegenerative disease. *Prion.* 9:90–109.
7. Jackrel, M. E., M. E. DeSantis, …, J. Shorter. 2014. Potentiated Hsp104 variants antagonize diverse proteotoxic misfolding events. *Cell.* 156:170–182.
8. Yasuda, K., S. F. Clatterbuck-Soper, …, S. Mili. 2017. FUS inclusions disrupt RNA localization by sequestering kinesin-1 and inhibiting microtubule detyrosination. *J. Cell Biol.* 216:1015–1034.
9. Tariq, A., J. Lin, …, J. Shorter. 2018. Potentiating Hsp104 activity via phosphomimetic mutations in the middle domain. *FEMS Yeast Res.* 18:1–14.
10. Doyle, S. M., and S. Wickner. 2009. Hsp104 and ClpB: protein disaggregating machines. *Trends Biochem. Sci.* 34:40–48.
11. Lum, R., M. Niggemann, and J. R. Glover. 2008. Peptide and protein binding in the axial channel of Hsp104. Insights into the mechanism of protein unfolding. *J. Biol. Chem.* 283:30139–30150.
12. Rajendar, B., and A. L. Lucius. 2010. Molecular mechanism of polypeptide translocation catalyzed by the Escherichia coli ClpA protein translocase. *J. Mol. Biol.* 399:665–679.
13. Miller, J. M., J. Lin, …, A. L. Lucius. 2013. E. coli ClpA catalyzed polypeptide translocation is allosterically controlled by the protease ClpP. *J. Mol. Biol.* 425:2795–2812.
14. Katayama, Y., S. Gottesman, …, M. R. Maurizi. 1988. The two-component, ATP-dependent Clp protease of Escherichia coli. Purification, cloning, and mutational analysis of the ATP-binding component. *J. Biol. Chem.* 263:15226–15236.
15. Gottesman, S., W. P. Clark, and M. R. Maurizi. 1990. The ATP-dependent Clp protease of Escherichia coli. Sequence of clpA and identification of a Clp-specific substrate. *J. Biol. Chem.* 265:7886–7893.
16. Hoskins, J. R., M. Pak, …, S. Wickner. 1998. The role of the ClpA chaperone in proteolysis by ClpAP. *Proc. Natl. Acad. Sci. USA.* 95:12135–12140.
17. Lee, D. H., and A. L. Goldberg. 2010. Hsp104 is essential for the selective degradation in yeast of polyglutamine expanded ataxin-1 but not most misfolded proteins generally. *Biochem. Biophys. Res. Commun.* 391:1056–1061.
18. Taxis, C., R. Hitt, …, D. H. Wolf. 2003. Use of modular substrates demonstrates mechanistic diversity and reveals differences in chaperone requirement of ERAD. *J. Biol. Chem.* 278:35903–35913.
19. Wallace, E. W., J. L. Kear-Scott, …, D. A. Drummond. 2015. Reversible, specific, active aggregates of endogenous proteins assemble upon heat stress. *Cell.* 162:1286–1298.
20. Tessarz, P., A. Mogk, and B. Bukau. 2008. Substrate threading through the central pore of the Hsp104 chaperone as a common mechanism for protein disaggregation and prion propagation. *Mol. Microbiol.* 68:87–97.
21. Castellano, L. M., S. M. Bart, …, J. Shorter. 2015. Repurposing Hsp104 to antagonize seminal amyloid and counter HIV infection. *Chem. Biol.* 22:1074–1086.
22. Weibezahn, J., P. Tessarz, …, B. Bukau. 2004. Thermotolerance requires refolding of aggregated proteins by substrate translocation through the central pore of ClpB. *Cell.* 119:653–665.
23. Li, T., C. L. Weaver, …, A. L. Lucius. 2015. Escherichia coli ClpB is a non-processive polypeptide translocase. *Biochem. J.* 470:39–52.
24. Yokom, A. L., S. N. Gates, …, D. R. Southworth. 2016. Spiral architecture of the Hsp104 disaggregase reveals the basis for polypeptide translocation. *Nat. Struct. Mol. Biol.* 23:830–837.
25. Gates, S. N., A. L. Yokom, …, D. R. Southworth. 2017. Ratchet-like polypeptide translocation mechanism of the AAA+ disaggregase Hsp104. *Science.* 357:273–279.
26. Deville, C., M. Carroni, …, H. R. Saibil. 2017. Structural pathway of regulated substrate transfer and threading through an Hsp100 disaggregase. *Sci. Adv.* 3:e1701726.
27. Yu, H., T. J. Lupoli, …, H. Li. 2018. ATP hydrolysis-coupled peptide translocation mechanism of Mycobacterium tuberculosis ClpB. *Proc. Natl. Acad. Sci. USA.* 115:E9560–E9569.
28. McClure, W. R., and Y. Chow. 1980. The kinetics and processivity of nucleic acid polymerases. *Methods Enzymol.* 64:277–297.
29. Lucius, A. L., N. K. Maluf, …, T. M. Lohman. 2003. General methods for analysis of sequential "n-step" kinetic mechanisms: application to single turnover kinetics of helicase-catalyzed DNA unwinding. *Biophys. J.* 85:2224–2239.
30. Lucius, A. L., J. M. Miller, and B. Rajendar. 2011. Application of the sequential n-step kinetic mechanism to polypeptide translocases. *Methods Enzymol.* 488:239–264.
31. Shorter, J., and S. Lindquist. 2005. Navigating the ClpB channel to solution. *Nat. Struct. Mol. Biol.* 12:4–6.
32. Haslberger, T., A. Zdanowicz, …, B. Bukau. 2008. Protein disaggregation by the AAA+ chaperone ClpB involves partial threading of looped polypeptide segments. *Nat. Struct. Mol. Biol.* 15:641–650.
33. Sweeny, E. A., M. E. Jackrel, …, J. Shorter. 2015. The Hsp104 N-terminal domain enables disaggregase plasticity and potentiation. *Mol. Cell.* 57:836–849.
34. Desantis, M. E., E. A. Sweeny, …, J. Shorter. 2014. Conserved distal loop residues in the Hsp104 and ClpB middle domain contact nucleotide-binding domain 2 and enable Hsp70-dependent protein disaggregation. *J. Biol. Chem.* 289:848–867.
35. Hoskins, J. R., S. Y. Kim, and S. Wickner. 2000. Substrate recognition by the ClpA chaperone component of ClpAP protease. *J. Biol. Chem.* 275:35361–35367.
36. Edelhoch, H. 1967. Spectroscopic determination of tryptophan and tyrosine in proteins. *Biochemistry.* 6:1948–1954.
37. Pace, C. N., F. Vajdos, …, T. Gray. 1995. How to measure and predict the molar absorption coefficient of a protein. *Protein Sci.* 4:2411–2423.
38. Weaver, C. L., E. C. Duran, …, A. L. Lucius. 2017. Avidity for polypeptide binding by nucleotide-bound Hsp104 structures. *Biochemistry.* 56:2071–2075.

39. Li, T., and A. L. Lucius. 2013. Examination of the polypeptide substrate specificity for Escherichia coli ClpA. *Biochemistry.* 52:4941–4954.

40. Doyle, S. M., J. Shorter, …, S. Wickner. 2007. Asymmetric deceleration of ClpB or Hsp104 ATPase activity unleashes protein-remodeling activity. *Nat. Struct. Mol. Biol.* 14:114–122.

41. Sweeny, E. A., M. E. Jackrel, …, J. Shorter. 2015. The Hsp104 N-terminal domain enables disaggregase plasticity and potentiation. *Mol. Cell.* 57:836–849.

42. Fischer, C. J., N. K. Maluf, and T. M. Lohman. 2004. Mechanism of ATP-dependent translocation of E.coli UvrD monomers along single-stranded DNA. *J. Mol. Biol.* 344:1287–1309.

43. Fischer, C. J., and T. M. Lohman. 2004. ATP-dependent translocation of proteins along single-stranded DNA: models and methods of analysis of pre-steady state kinetics. *J. Mol. Biol.* 344:1265–1286.

44. Ali, J. A., and T. M. Lohman. 1997. Kinetic measurement of the step size of DNA unwinding by Escherichia coli UvrD helicase. *Science.* 275:377–380.

45. Lucius, A. L., A. Vindigni, …, T. M. Lohman. 2002. DNA unwinding step-size of E. coli RecBCD helicase determined from single turnover chemical quenched-flow kinetic studies. *J. Mol. Biol.* 324:409–428.

46. Lucius, A. L., C. J. Wong, and T. M. Lohman. 2004. Fluorescence stopped-flow studies of single turnover kinetics of E.coli RecBCD helicase-catalyzed DNA unwinding. *J. Mol. Biol.* 339:731–750.

47. Jankowsky, E., C. H. Gross, …, A. M. Pyle. 2000. The DExH protein NPH-II is a processive and directional motor for unwinding RNA. *Nature.* 403:447–451.

48. Li, T., J. Lin, and A. L. Lucius. 2015. Examination of polypeptide substrate specificity for Escherichia coli ClpB. *Proteins.* 83:117–134.

49. Otto, M. R., M. P. Lillo, and J. M. Beechem. 1994. Resolution of multiphasic reactions by the combination of fluorescence total-intensity and anisotropy stopped-flow kinetic experiments. *Biophys. J.* 67:2511–2521.

50. Jackrel, M. E., and J. Shorter. 2014. Potentiated Hsp104 variants suppress toxicity of diverse neurodegenerative disease-linked proteins. *Dis. Model. Mech.* 7:1175–1184.

51. Franzmann, T. M., A. Czekalla, and S. G. Walter. 2011. Regulatory circuits of the AAA+ disaggregase Hsp104. *J. Biol. Chem.* 286:17992–18001.

52. Kłosowska, A., T. Chamera, and K. Liberek. 2016. Adenosine diphosphate restricts the protein remodeling activity of the Hsp104 chaperone to Hsp70 assisted disaggregation. *Elife.* 5:e15159.

53. DeSantis, M. E., E. H. Leung, …, J. Shorter. 2012. Operational plasticity enables hsp104 to disaggregate diverse amyloid and nonamyloid clients. *Cell.* 151:778–793.

54. Torrente, M. P., L. M. Castellano, and J. Shorter. 2014. Suramin inhibits Hsp104 ATPase and disaggregase activity. *PLoS One.* 9:e110115.

55. De Los Rios, P., A. Ben-Zvi, …, P. Goloubinoff. 2006. Hsp70 chaperones accelerate protein translocation and the unfolding of stable protein aggregates by entropic pulling. *Proc. Natl. Acad. Sci. USA.* 103:6166–6171.

56. Shorter, J., and S. Lindquist. 2004. Hsp104 catalyzes formation and elimination of self-replicating Sup35 prion conformers. *Science.* 304:1793–1797.

57. Lo Bianco, C., J. Shorter, …, P. Aebischer. 2008. Hsp104 antagonizes alpha-synuclein aggregation and reduces dopaminergic degeneration in a rat model of Parkinson disease. *J. Clin. Invest.* 118:3087–3097.

58. Shorter, J., and S. Lindquist. 2008. Hsp104, Hsp70 and Hsp40 interplay regulates formation, growth and elimination of Sup35 prions. *EMBO J.* 27:2712–2724.

59. Schaupp, A., M. Marcinowski, …, S. Walter. 2007. Processing of proteins by the molecular chaperone Hsp104. *J. Mol. Biol.* 370:674–686.

60. Wendler, P., J. Shorter, …, H. R. Saibil. 2007. Atypical AAA+ subunit packing creates an expanded cavity for disaggregation by the protein-remodeling factor Hsp104. *Cell.* 131:1366–1377.

61. Heuck, A., S. Schitter-Sollner, …, T. Clausen. 2016. Structural basis for the disaggregase activity and regulation of Hsp104. *Elife.* 5:e21516.

62. Durie, C. L., E. C. Duran, and A. L. Lucius. 2018. Escherichia coli DnaK allosterically modulates ClpB between high and low peptide affinity states. *Biochemistry.* 57:3665–3675.

63. Rosenzweig, R., S. Moradi, …, L. E. Kay. 2013. Unraveling the mechanism of protein disaggregation through a ClpB-DnaK interaction. *Science.* 339:1080–1083.

64. Doyle, S. M., S. Shastry, …, S. Wickner. 2015. Interplay between E. coli DnaK, ClpB and GrpE during protein disaggregation. *J. Mol. Biol.* 427:312–327.

65. Miot, M., M. Reidy, …, S. Wickner. 2011. Species-specific collaboration of heat shock proteins (Hsp) 70 and 100 in thermotolerance and protein disaggregation. *Proc. Natl. Acad. Sci. USA.* 108:6915–6920.

66. Oguchi, Y., E. Kummer, …, B. Bukau. 2012. A tightly regulated molecular toggle controls AAA+ disaggregase. *Nat. Struct. Mol. Biol.* 19:1338–1346.

67. Seyffer, F., E. Kummer, …, A. Mogk. 2012. Hsp70 proteins bind Hsp100 regulatory M domains to activate AAA+ disaggregase at aggregate surfaces. *Nat. Struct. Mol. Biol.* 19:1347–1355.

68. Hoskins, J. R., S. M. Doyle, and S. Wickner. 2009. Coupling ATP utilization to protein remodeling by ClpB, a hexameric AAA+ protein. *Proc. Natl. Acad. Sci. USA.* 106:22233–22238.

Biophysical Journal, Volume *116*

Supplemental Information

Hsp104 and Potentiated Variants Can Operate as Distinct Nonprocessive Translocases

Clarissa L. Durie, JiaBei Lin, Nathaniel W. Scull, Korrie L. Mack, Meredith E. Jackrel, Elizabeth A. Sweeny, Laura M. Castellano, James Shorter, and Aaron L. Lucius

Supplementary Data

Fluorescence of fluorescein labeled RepA peptide is quenched upon binding by Hsp104

In previous studies of ClpA and ClpB, the fluorescence of fluorescein-labeled peptides was observed to be quenched when the peptide was bound by the much larger hexameric motor protein.[1-3] The sequences of those peptides differ from that of our RepA truncation peptides. In a recent study of Hsp104 peptide binding in the presence of various nucleotide analogues, quenching of the peptide was observed upon $RepA_{Flu1-50}$ binding by Hsp104 in the presence of ATPγS.[4] Here, we tested for fluorescence quenching with other RepA truncation peptides as schematized in Figure 1 A. In Supplementary Figure 1 B the maximum fluorescence emission of $RepA_{1-30Flu}$ was reduced by approximately 20% in the presence of Hsp104 and ATPγS, conditions in which Hsp104 avidly binds RepA truncation peptides. This observation is consistent with previous studies using this experimental design.

Simulations of predicted time courses

We simulated predicted time courses for the ATP dependent translocation of polypeptide substrates by Hsp104, based on the model proposed from the recent CryoEM reconstruction of Hsp104 bound to peptide. Supplemental Figures 2 A, B, and C show the time courses predicted for processive translocation of a 30, 40, and 50 amino acid peptide in three possible scenarios. Figure S2A represents the predicted time courses if Hsp104 translocates peptide from one end to the other, as schematized in Figure 1 C and D. Note the presence of a lag that depends on the length of the polypeptide. Figure S2B represents the predicted time courses if Hsp104 translocates from the middle of the polypeptide to one end, as schematized in Figure 1 E and F. A peptide length dependent lag is observed in these time courses as well. Finally, in Figure S2C, the predicted time courses are for a scenario in which Hsp104 binds an end of the polypeptide and that translocates directly off that end. Here, a lag is observed but that lag is not dependent on the length of the polypeptide. These simulations use the reported ATPase rate constant of 10 min^{-1}.[5] Though the rate constant could differ from the ATPase rate constant, they are expected to be similar as ATP binding and hydrolysis is coupled to polypeptide translocation. With this rate constant, the simulation (Supplemental Figure 2C) shows that a lag of approximately 15 seconds when the minimum number of steps (7) is taken to translocate the bound peptide out of the Hsp104 axial channel.

Kinetic parameters do not vary with Hsp104 concentration

Based on Binding Density Function studies of the Hsp104 bacterial homologue ClpB[6], we selected peptide lengths (30, 40, 50, 102, and 127 amino acids) that were expected to accommodate no more than one Hsp104 hexamer. To test this, we applied the same experimental design as schematized in Figure 1B with lower concentrations of Hsp104. In syringe 1, complex was assembled with 200 nM, 1 μM, 2 μM (the concentration used throughout this manuscript), or 4 μM Hsp104, 20 nM $RepA_{1-50Flu}$, and 300 mM ATPγS. If all of the Hsp104 assembled into hexamers, the concentration of Hsp104 would be 33 nM, 167 nM, 333 nM, or 667 nM, relative to 20 nM peptide. These concentrations represent an upper limit. Hsp104 exists in an equilibrium of

oligomers. The concentration of Hsp104 hexamers ranges from 1.65 to 33 fold excess to peptide. The kinetic parameters, summarized in Supplemental Table 1 are similar across this range, indicating that the number of Hsp104 hexamers bound to the peptide does not vary with Hsp104 concentration, suggesting there cannot be more than one hexamer on these lengths of peptide simultaneously.

A lag in dissociation time courses is not observed in the absence of ATP

In the main manuscript, Figure 2A shows that Hsp104-peptide complex dissociates upon rapid mixing with ATP. Each time course exhibits a lag followed by an increase in signal. To confirm that the lag was due to kinetic steps linked to ATP binding and hydrolysis, we repeated the experiments mixing the complex with buffer alone or with casein trap. The time courses, displayed in Supplemental Figure 3, show that no lag was observed in the experiments where ATP was not included. These time courses proceed on a longer time scale than those in Figure 2, consistent with the understanding that dissociation follows ATP-dependent steps.

Hsp104 does not exhibit length dependence on substrates greater than 100 amino acids in length

Stopped flow anisotropy experiments were carried out by pre-mixing 2 μM Hsp104 with either α-casein 102 or 127 fluorescently modified at the N-terminus with fluorescein, and 300 μM ATPγS. This sample was loaded into one syringe of the stopped-flow. In the other syringe was 10 mM ATP and 20 μM unmodified α-casein to serve as a trap for any unbound Hsp104. The two reactants were rapidly mixed and anisotropy and total fluorescence were simultaneously collected. The two time courses (anisotropy and total fluorescence) were simultaneously subjected to global NLLS analysis using equations 36 and 37 for Scheme 3 as described in the supplemental methods. The dashed black lines in supplemental Figure 4 A – D are the result of the global analysis to Scheme 3. The data are well described by this model. Most importantly, the parameters are in agreement with the parameters determined from the analysis of the data presented in Figure 3 for the RepA peptide (see parameters in supplemental Figure 4 legend).

To establish whether all of the Hsp104 is dissociating from the polypeptide chain α-casein 102 and 127 were rapidly mixed against buffer. These time course are shown in supplemental Figure 4A and B as a dashed colored line. Since no change was observed these time courses were only collected over 100 s. For α-casein 102 the value of the anisotropy over 100 s was $\langle r \rangle = 0.1193 \pm 0.0006$ and for α-casein 127, $\langle r \rangle = 0.1472 \pm 0.0005$. As can be seen in supplemental Figure 4A and B the time courses are approaching the average value of the anisotropy for the peptide alone. Further, the final anisotropy predicted from the NLLS analysis yielded $r_P = 0.114 \pm 0.002$ and $r_P = 0.147 \pm 0.002$ for a-casein 102 and 127, respectively. These observations are consistent with all of the Hsp104 dissociating from the polypeptide.

Processive translocase ClpA exhibits length dependence on substrates greater than 100 amino acids in length

Supplementary Figure 5 shows a representative set of fluorescence anisotropy time courses collected with fluorescein labeled 102 amino acid (orange trace) and 127 amino acid (red trace) truncations of αS1-casein. The time courses from ClpA catalyzed translocation reveal a high initial

anisotropy, consistent with the fluorescently labeled substrate bound by the respective hexameric motors, followed by a decrease in anisotropy over time after rapid mixing with ATP and a protein trap, consistent with dissociation of the substrate from the hexameric motor. Unlike our observations in Figure 2C, the ClpA time courses reveal a length dependent lag prior to dissociation. Our observation here is consistent with previous reports[3] of a substrate length dependent lag in translocation of substrate by the processive translocase ClpA.

Hsp104 does not exhibit directional preference

In order to test whether Hsp104 exhibits a directional preference for translocation with respect to the peptide, we repeated the experiments in Figure 2 A-C with peptides that had been labeled on the C terminus, rather than the N terminus. The dissociation time courses for $RepA_{1\text{-}30Flu}$, $RepA_{1\text{-}40Flu}$, and $RepA_{1\text{-}50Flu}$ were fit to Scheme 1 as described in the main text. The resulting parameters are summarized in Supplemental Table 2 (compare to Table 2 in the main manuscript) and the *n* vs *l* plot is shown in Supplemental Figure 6A, green squares. No length dependence trend is observed with respect to the number of kinetic steps. In Supplemental Figure 6A, the gray circles are the number of steps observed with the N terminally labeled RepA truncation peptides reported in Figure 2B.

The anisotropy experiment was also performed with C terminally labeled 127 amino acid truncation of casein, Supplemental Figure 6 B, to assess whether a directional preference would be exhibited with longer substrates. We observed that the time course from the C labeled substrate (green) was not different from the time course obtained with the N labeled substrate (grey).

Residuals of Fitting Translocation Data with Scheme 2

Figure 3 shows representative ATP dependent Hsp104-catalyzed polypeptide translocation time courses. Each color corresponds to a different ATP concentration, with 10 μM ATP shown in red. Intermediate concentrations of ATP go through orange, green, and blue, with the highest concentration, 5 mM ATP, shown in purple. The broken black traces represent the best fit lines of each time course, individually, to the equation derived from Scheme 2 using NLLS analysis. To further assess how well Scheme 2 describes the data, Supplemental Figure 7 shows the same time courses presented in Figure 3 on a log scale, along with the residuals of the fits shown in Figure 3. The residuals are small, indicating that the data are well described by Scheme 2.

ATPγS Concentration Effect on Translocation Time Courses

Our recent work showed that assembly of the Hsp104-peptide complex requires the presence of ATPγS; other commonly used nucleotide analogues do not support avid peptide binding. Doyle *et al*. previously observed that a 3:1 ratio of ATP:ATPγS "unleashes" the activity of Hsp104.[5] Because both ATPγS and ATP are required in the present experimental design, we sought to test whether, or to what degree, the amounts of ATPγS and ATP used in our experiments affect our observations.

First, we tested the 3 mM ATP and 1 mM ATPγS in the reaction. These are the nucleotide concentrations used in Doyle *et al*. for Hsp104 activity assays including RepA activation, heat-aggregated GFP reactivation, $RepA_{1-70}GFP$ unfolding assays, and ATPase assays. The time course is displayed in Supporting Figure 8 A, purple, solid trace. We observed that the time course was well described by Scheme 2 (variance $4.4x10^{-6}$). The fit is overlaid with the time course in a broken black line in Supporting Figure 8 A. We can compare the time course and best fit parameters to our time courses produced by 3 mM ATP in the presence of 150 μM ATPγS (representative time course shown in pink solid trace with fit line to Scheme 2 overlaid in black broken line, Figure 8 A). Comparing the time courses with 3 mM ATP, the time course collected with a 3:1 ratio of ATP:ATPγS (purple trace) is slower than that from our standard assay with 150 μM ATPγS. This is consistent with the idea of the slowly hydrolysable ATP analogue acting as an inhibitor to the ATP dependent reaction, however upon introduction and analysis of data from the potentiated variant Hsp104A503S (Figure 4 in the main text) we will propose a more nuanced interpretation. The best fit parameters summarized in Supplementary Table 3 show that the rate constants for k_{np} and $k_{obs,1}$ in the 3:1 or optimal activity condition, as identified by Doyle, *et al*., are both significantly slower than k_{np} and $k_{obs,1}$ in our standard assay. In contrast, the rate constant for $k_{obs,2}$ is similar in the 3:1 condition.

Next, we selected a condition in which we could maintain the 3:1 ATP:ATPγS ratio and also make a direct comparison to total nucleotide concentration in one of our standard reaction conditions. Of our standard experimental conditions, the 300 μM and 700 μM ATP experiments were closest to the 3:1 ATP:ATPγS ratio. Our standard reaction conditions contain 150 μM ATPγS upon mixing equal volumes of the contents of the incubation syringes (See Figure 1B, main text). The 300 μM ATP standard condition results in a 2:1 ATP:ATPγS ratio and the 700 μM ATP standard condition results in a ~5:1 ATP: ATPγS. Figure 1d in Doyle *et al.* shows a steep transition in the curve of ClpB catalyzed RepA activation as a function of ATP/ATPγS, on either side of the maximally active ratio.[5] If the curve for Hsp104 activity as a function of ATP:ATPγS has a similar shape, we would expect to observe a notable difference in the time courses collected by adjusting the nucleotide ratio in this range. We chose a total nucleotide concentration of 850 μM, with the 3:1 ATP:ATPγS condition requiring 637.5 μM ATP and 212.5 μM ATPγS. This time course is displayed in Supporting Figure 8 B (purple solid trace). A representative time course from the standard condition with 700 μM ATP and 150 μM ATPγS is included in Supporting Figure 8 B (pink solid trace) for direct comparison of these conditions. The effect is less pronounced here than in Supporting Figure 8 A. Qualitatively, the 3:1 ratio of ATP:ATPγS (purple trace) condition is slower than that from our standard assay with 150 μM ATPγS. Both time courses were fit to Scheme 2 (black broken traces). Each of the parameters, summarized in Supporting Table 3, are within one to two standard deviations for these conditions. We did not observe a significant effect in this nucleotide concentration range by varying the ATP:ATPγS ratio. As discussed in the main text, we propose that the differences in experimental design between the current study and the Doyle et al work investigate different aspects of the Hsp104 mechanism.

Rapid Mixing Experiments with Fluorescein-Modified α-Casein Truncation Peptides

Experiments were performed using an Applied Photophysics SX20 stopped flow fluorometer as described above with the additional use of the Fluorescence Polarisation Accessory. Two R-6095 photomultiplier tubes were used, each with a 515 nm cut off long pass filter. One syringe of the stopped flow fluorometer contained a solution of fluorescein labeled α-casein peptide (20 nM), Hsp104 (2 μM), and ATPγS (300 μM). The other syringe contained a solution of 10 mM ATP and 20 μM α-casein. The solutions were loaded, separately, into the stopped flow fluorimeter. The solutions were rapidly mixed. Experiments were replicated.

NLLS Analysis of Transient State Kinetics

Averaged time courses were normalized to begin at a fluorescence intensity of zero and end at a fluorescence intensity of 1.

For analysis of substrate-length dependence, the system of coupled differential equations that result from Scheme 1 was solved using the method of Laplace transforms to obtain an expression for substrate release as a function of the Laplace variable, *S(s)*, given by Eq. (1):

$$S(s) = \frac{1}{s} \bullet \frac{(k_{np} + sx)}{(k_{np} + s)} \bullet \left(\frac{k_t}{k_t + s} \right)^n \tag{1}$$

where *S* represents the substrate and *s* is the Laplace variable, *n* is the number of steps with rate constant k_t (see Fischer and Lohman [7] for a discussion of non-integer values for *n*), k_{np} is the rate constant of transition from a nonproductive to a productive complex, and *x* is the fraction of Hsp104 bound to polypeptide in the productive form of the complex, given by Eq (2):

$$x = \frac{[C]}{[C] + [C^*]} \tag{2}$$

For analysis of ATP dependence, the system of coupled differential equations that result from Scheme 2 was solved using the method of Laplace transforms to obtain an expression for substrate release as a function of the Laplace variable, *S(s)*, given by Eq. (3):

$$S(s) = \frac{1}{s} \bullet \frac{(k_{np} + sx)}{(k_{np} + s)} \bullet \frac{k_{obs,1} \bullet k_{obs,s}}{(k_{obs,1} + s)(k_{obs.2} + s)} \tag{3}$$

where $k_{obs,1}$ and $k_{obs,2}$ are separate rate constants. All other variables are the same as described above.

For analysis of the Hsp104A503S data, the system of coupled differential equations that result from Scheme 3 was solved using the method of Laplace transforms to obtain an expression for substrate release as a function of the Laplace variable, *S(s)*, given by Eq. (4)

$$S(s) = \frac{1}{s} \bullet \frac{(k_{np} + sx)}{(k_{np} + s)} \bullet \frac{k_{obs,1}}{(k_{obs,1} + s)} \tag{4}$$

Equations (1), (3), and (4) were numerically solved using Equation (5) to describe substrate release as a function of time, $S(t)$:

$$S(t) = A_T \mathcal{L}^{-1} S(s) \tag{5}$$

Where A_T is the total amplitude of the time course, and $\mathcal{L}^{-1}$ is the inverse Laplace transform operator. This was performed using the non-linear least squares (NLLS) fitting routine, Conlin, kindly provided by Dr. Jeremy Williams[8], and the inverse Laplace transform function using the IMSL C Numerical Libraries from Visual Numerics (Houston, TX), as previously described.[1, 2]

The ATP concentration dependence of the rate constants displayed in Figures 4 D, and 6 E & F was subjected to NLLS analysis using a rectangular hyperbola as given by Equation (6):

$$k_{obs,x} = \frac{k_{obs,x,max}[ATP]}{K_{1/2} + [ATP]} \tag{6}$$

Derivation of Equations for NLLS Analysis

In Scheme 1, Hsp104 is prebound to the polypeptide in both a productive form C and a non-productive form C^*, respectively, which accounts for the biphasic kinetics observed. Upon rapid mixing with ATP, Hsp104 can translocate the polypeptide with rate k_t, forming an intermediate complex I. This kinetic step with rate constant k_t can be repeated n times before Hsp104 dissociates from the peptide, P. The system of coupled differential equations describing Scheme 1 are given below.

$$\frac{\delta C^*}{\delta t} = -k_{np}[C^*] \tag{7}$$

$$\frac{\delta C}{\delta t} = k_{np}[C^*] - k_t[C] \tag{8}$$

$$\frac{\delta I_1}{\delta t} = k_t[C] - k_t[I_1] \tag{9}$$

$$\frac{\delta I_{2<i<n-1}}{\delta t} = k_t[I_{i-1}] - k_t[I_i] \tag{10}$$

$$\frac{\delta P}{\delta t} = k_t[I_{n-1}] \tag{11}$$

The Laplace transform was applied to this series of coupled differential equations, resulting in the series of coupled algebraic equations below (see Reference [9] for more detail).

$$(s + k_{np})C^*'(s) = C^*(0) \tag{12}$$

$$-k_{np}C^*'(s) + (s + k_t)C'(s) = C(0) \tag{13}$$

$$-k_t C'(s) + (s + k_t)I_1'(s) = 0 \tag{14}$$

$$-k_t I_{i-1}'(s) + (s + k_t)I_i'(s) = 0 \tag{15}$$

$$-k_t I_n'(s) + sP'(s) = 0 \tag{16}$$

where $C^{*\prime}(s)$, $C'(s)$, $I_n'(s)$, and $P'(s)$ represent the concentrations of substrate-enzyme complex (nonproductive and productive forms), intermediate, and product, respectively, as functions of the complex Laplace variable s. C*(0) and C(0) are the initial concentrations of the complex in the nonproductive and productive forms, respectively, at time $t = 0$. We have assumed at time there is no population of any intermediate or product to which our assay is sensitive.

These equations can be written in matrix form as

$$\begin{pmatrix} s+k_{np} & 0 & 0 & \cdots & 0 & \cdots & 0 & 0 \\ -k_{np} & s+k_t & 0 & \cdots & 0 & \cdots & 0 & 0 \\ 0 & -k_t & s+k_t & \cdots & 0 & \cdots & 0 & 0 \\ \vdots & \vdots & \vdots & \ddots & 0 & \cdots & 0 & 0 \\ 0 & 0 & 0 & -k_t & s+k_t & \cdots & 0 & 0 \\ \vdots & \vdots & \vdots & \vdots & \vdots & \ddots & 0 & 0 \\ 0 & 0 & 0 & 0 & 0 & -k_t & s+k & 0 \\ 0 & 0 & 0 & 0 & 0 & 0 & -k_t & s \end{pmatrix} \begin{pmatrix} C^*'(s) \\ C'(s) \\ I_1(s) \\ \vdots \\ I_i'(s) \\ \vdots \\ I_n'(s) \\ P'(s) \end{pmatrix} = \begin{pmatrix} C^*(0) \\ C(0) \\ 0 \\ \vdots \\ 0 \\ \vdots \\ 0 \\ 0 \end{pmatrix} \tag{17}$$

Since C*(0) and C(0) are constants they can be replaced using Equation (2) as the fraction of productively bound complexes, x, and teh fraction of non-productively bound complexes, (1 – x). Equation (17) can be represented as Equation (18).

$$\begin{pmatrix} s+k_{np} & 0 & 0 & \cdots & 0 & \cdots & 0 & 0 \\ -k_{np} & s+k_t & 0 & \cdots & 0 & \cdots & 0 & 0 \\ 0 & -k_t & s+k_t & \cdots & 0 & \cdots & 0 & 0 \\ \vdots & \vdots & \vdots & \ddots & 0 & \cdots & 0 & 0 \\ 0 & 0 & 0 & -k_t & s+k_t & \cdots & 0 & 0 \\ \vdots & \vdots & \vdots & \vdots & \vdots & \ddots & 0 & 0 \\ 0 & 0 & 0 & 0 & 0 & -k_t & s+k & 0 \\ 0 & 0 & 0 & 0 & 0 & 0 & -k_t & s \end{pmatrix} \begin{pmatrix} C^*'(s) \\ C'(s) \\ I_1(s) \\ \vdots \\ I_i'(s) \\ \vdots \\ I_n'(s) \\ P'(s) \end{pmatrix} = \begin{pmatrix} (1-x) \\ x \\ 0 \\ \vdots \\ 0 \\ \vdots \\ 0 \\ 0 \end{pmatrix} \tag{18}$$

The matrices can then be row reduced as below, where each term in the last column is the Laplace transform or the concentration of each species in Scheme 1.

$$\begin{pmatrix} 1 & 0 & 0 & \cdots & 0 & \cdots & 0 & 0 \\ 0 & 1 & 0 & \cdots & 0 & \cdots & 0 & 0 \\ 0 & 0 & 1 & \cdots & 0 & \cdots & 0 & 0 \\ \vdots & \vdots & \vdots & \ddots & 0 & \cdots & 0 & 0 \\ 0 & 0 & 0 & 0 & 1 & \cdots & 0 & 0 \\ \vdots & \vdots & \vdots & \vdots & \vdots & \ddots & 0 & 0 \\ 0 & 0 & 0 & 0 & 0 & 0 & 1 & 0 \\ 0 & 0 & 0 & 0 & 0 & 0 & 0 & 1 \end{pmatrix} \begin{pmatrix} C^*'(s) \\ C'(s) \\ I_1(s) \\ \vdots \\ I_i'(s) \\ \vdots \\ I_n'(s) \\ P'(s) \end{pmatrix} = \begin{pmatrix} \dfrac{1-x}{k_{np}+s} \\ \dfrac{k_{np}+sx}{\left(k_{np}+s\right)\left(k_t+s\right)} \\ \dfrac{\left(k_{np}+sx\right)k_t}{\left(k_{np}+s\right)\left(k_t+s\right)^2} \\ \vdots \\ \dfrac{\left(k_{np}+sx\right){k_t}^i}{\left(k_{np}+s\right)\left(k_t+s\right)^{i+1}} \\ \vdots \\ \dfrac{{k_t}^{n-1}\left(k_{np}+sx\right)}{\left(k_{np}+s\right)\left(k_t+s\right)^n} \\ \dfrac{{k_t}^n\left(k_{np}+sx\right)}{s\left(k_{np}+s\right)\left(k_t+s\right)^n} \end{pmatrix} \tag{19}$$

Note that the expression for substrate release as a function of the Laplace variable, S(s), given by Eq. (1) is the same as the bottom entry in the last column above. The time-dependent expression for the concentrations of substrate release was obtained by taking the inverse Laplace transform of that equation using the mathematical software package Mathematica.

The same strategy as outlined above was followed for obtaining the time dependent expression for the release of substrate using Eq (3). In Scheme 2, as in Schemes 1, Hsp104 is prebound to the polypeptide in both a productive form *C* and a non-productive form *C**, respectively, which accounts for the biphasic kinetics observed. Upon rapid mixing with ATP, Hsp104 translocates the polypeptide with rate constant $k_{obs,1}$, forming an intermediate complex *I*. The intermediate goes through second kinetic step with rate constant $k_{obs,2}$, resulting in Hsp104 dissociation from the peptide, *P*. The system of coupled differential equations describing Scheme 2 are given below.

$$\frac{\delta[C^*]}{\delta t} = -k_{np}\left[C^*\right] \tag{20}$$

$$\frac{\delta[C]}{\delta t} = k_{np}\left[C^*\right] - k_{obs,1}\left[C\right] \tag{21}$$

$$\frac{\delta[I]}{\delta t} = k_{obs,1}\left[C\right] - k_{obs,2}\left[I\right] \tag{22}$$

$$\frac{\delta[P]}{\delta t} = k_{obs,2}\left[I\right] \tag{23}$$

The Laplace transform was applied to this series of coupled differential equations, resulting in the series of coupled algebraic equations below

$$(s + k_{np})C^{*}{}'(s) = C^{*}(0) \tag{24}$$

$$-k_{np}C^{*}{}'(s) + (s + k_{obs,1})C'(s) = C(0) \tag{25}$$

$$-k_{obs,1}C'(s) + (s + k_{obs,2})I'(s) = 0 \tag{26}$$

$$-k_{obs,2}I'(s) + sP'(s) = 0 \tag{27}$$

Where the variables are as described above. As with Scheme 1, we have assumed at time there is no population of any intermediate or product to which our assay is sensitive.

These equations can be written in matrix form as

$$\begin{pmatrix} 1 & 0 & 0 & 0 \\ 0 & 1 & 0 & 0 \\ 0 & 0 & 1 & 0 \\ 0 & 0 & 0 & 1 \end{pmatrix} \begin{pmatrix} C^{*\prime}(s) \\ C^{\prime}(s) \\ I^{\prime}(s) \\ P^{\prime}(s) \end{pmatrix} = \begin{pmatrix} \dfrac{1-x}{k_{np}+s} \\ \dfrac{k_{np}+sx}{\left(k_{np}+s\right)\left(k_{obs,1}+s\right)} \\ \dfrac{\left(k_{np}+sx\right)k_{obs,1}}{\left(k_{np}+s\right)\left(k_{obs,1}+s\right)\left(k_{obs,2}+s\right)} \\ \dfrac{\left(k_{np}+sx\right)k_{obs,1}k_{obs,2}}{s\left(k_{np}+s\right)\left(k_{obs,1}+s\right)\left(k_{obs,2}+s\right)} \end{pmatrix} \tag{28}$$

Note that the expression for substrate release as a function of the Laplace variable, S(s), given by Eq. (6) is the same as the bottom entry in the last column above. The time-dependent expression for the concentrations of substrate release was obtained by taking the inverse Laplace transform of that equation, again using the mathematical software package Mathematica.

The same strategy as outlined above was followed again for obtaining the time dependent expression for the release of substrate using Eq (7). In Scheme 3, as in Schemes 1 and 2, Hsp104 can be prebound to the polypeptide in both a productive form *C* and a non-productive form *C**. Upon rapid mixing with ATP, Hsp104 translocates the polypeptide with rate constant $k_{obs,1}$, resulting in Hsp104 dissociation from the peptide, *P*. The system of coupled differential equations describing Scheme 3 are given below include Equations (22) and (23) as well as Equation (31) below.

$$\frac{\delta[P]}{\delta t} = k_{obs,1}\left[C\right] \tag{29}$$

The Laplace transform was applied to this series of coupled differential equations, resulting in the series of coupled algebraic Equations (23), (27) and (32) below

$$-k_{obs,1}C^{\prime}(s) + sP^{\prime}(s) = 0 \tag{30}$$

Where the variables are as described above. As with Schemes 1 and 2, we have assumed at time there is no population of any intermediate or product to which our assay is sensitive.

These equations can be written in matrix form as

$$\begin{pmatrix} 1 & 0 & 0 \\ 0 & 1 & 0 \\ 0 & 0 & 1 \end{pmatrix} \begin{pmatrix} C^{*\prime}(s) \\ C^{\prime}(s) \\ P^{\prime}(s) \end{pmatrix} = \begin{pmatrix} \dfrac{1-x}{k_{np}+s} \\ \dfrac{k_{np}+sx}{(k_{np}+s)(k_{obs,1}+s)} \\ \dfrac{\left(k_{np}+sx\right)k_{obs,1}}{s(k_{np}+s)(k_{obs,1}+s)} \end{pmatrix} \quad (31)$$

Note that the expression for substrate release as a function of the Laplace variable, S(s), given by Eq. (7) is the same as the bottom entry in the last column above. The time-dependent expression for the concentrations of substrate release was obtained by taking the inverse Laplace transform of that equation, again using the mathematical software package Mathematica.

NLLS Analysis of Anisotropy Stopped Flow Data

The anisotropy time courses were subjected to NLLS analysis using the strategy described by Otto et al (19). Unlike fluorescence, an anisotropy time course is not described by only changes in anisotropy. Rather, there can be effects on the anisotropy due to quantum yield changes. Since the raw fluorescence time courses we report here exhibit a fluorescence change upon Hsp104 dissociation the total intensity is also expected to exhibit changes, where total intensity is given by

$$I_{total} = I_{VV} + 2GI_{VH} \quad 32$$

And anisotropy is given by

$$r = \frac{I_{VV} - GI_{VH}}{I_{VV} + 2GI_{VH}} \quad 33$$

Thus, the time dependence of the total intensity is given by

$$I_{total}(t) = \sum x_i(t) q_i^{eff} \quad 34$$

And the time dependence of the anisotropy is given by

$$r(t) = \frac{\sum x_i(t) q_i^{eff} r_i}{\sum x_i(t) q_i^{eff}} \quad 35$$

Where, $x_i(t)$ represent the i-th species in the reaction and q_i^{eff} is the effective quantum yield for the i-th species, and r_i is the anisotropy for the i-th species.

For scheme 3 equation 34 and 35 would be given by

$$I_{total}(t) = C^*(t) q_{CS}^{eff} r_{CS} + C(t) q_C^{eff} r_C + I(t) q_I^{eff} r_I + P(t) q_P^{eff} r_P \quad 36$$

$$r(t) = \frac{C^*(t) q_{CS}^{eff} r_{CS} + C(t) q_C^{eff} r_C + I(t) q_I^{eff} r_I + P(t) q_P^{eff} r_P}{C^*(t) q_{CS}^{eff} + C(t) q_C^{eff} + I(t) q_I^{eff} + P(t) q_P^{eff}} \quad 37$$

Where each time dependent function in equations 36 – 37 is determined by finding the inverse Laplace transform of the functions in Equation (28) of the manuscript.

Hsp104 dissociation was well described by equation 36 and 37 using Scheme 3 in the manuscript. The effective quantum yields and the anisotropies were determined for each species. The bound complexes (C*, C, and I) all exhibit similar quantum yields and anisotropy values whereas, free peptide, P, exhibits a different quantum yield and anisotropy, consistent with dissociation. This is consistent with our previous interpretation that the signal change arises from release of the polypeptide chain.

Supplemental Figure 4 A and B show the anisotropy time courses with their associated fits for a-casein 102 and 127, respectively. Figure 4 C and D show the corresponding total fluorescence time courses that were simultaneously collected with the anisotropy data. The anisotropy and total fluorescence time courses were simultaneously fit using equations 36 and 37.

Supplementary Figure Legends

Supplementary Figure 1 Fluorescence quenching controls. (A) Schematic for quenching control. 100 nM $RepA_{1\text{-}30Flu}$ was in a fluorescence cuvette at 25 °C. ATPγS and, subsequently, Hsp104 were added to the cuvette. (B) Emission spectra of $RepA_{1\text{-}30Flu}$ upon excitation at 494 nm. Green solid line represents $RepA_{1\text{-}30Flu}$ in the absence of peptide or protein. Orange broken line represents $RepA_{1\text{-}30Flu}$ in the presence of ATPγS. Purple dotted line represents $RepA_{1\text{-}30Flu}$ in the presence of ATPγS and Hsp104. Final concentrations are 100 nM $RepA_{1\text{-}30Flu}$, 300 μM ATPS, and 2 μM Hsp104. Spectra have been corrected for dilution. Fluorescence intensity is reported in arbitrary units (A. U.).

Supplementary Figure 2. Simulated time courses. A series of time courses have been simulated for the processive translocation of 30, 40, and 50 amino acid polypeptides. The simulation uses a previously reported ATPase rate constant for Hsp104[5] and the recently proposed mechanistic model based on CryoEM reconstructions with translocation steps of 2 amino acids resulting from the closed to extended conformational changes of the Hsp104 hexamer, linked to the ATP binding and hydrolysis cycle.[10] The simulations in Panel A represent the scenario in which Hsp104 binds at one end of the polypeptide and translocates to the other end, as schematized in Figure 1C &D. Panel B represents the time courses predicted when Hsp104 binds in the middle of polypeptide and translocates to an end as schematized in Figure 1E&F. The simulations in Panel C represent a scenario in which Hsp104 binds to an end of the polypeptide and translocates off that end.

Supplementary Figure 3. Complex dissociation upon mixing with buffer or casein trap. Hsp104 or $Hsp104^{A503S}$ (2 μM), ATPγS (300 μM), and fluorescently labeled RepA truncation peptide (20 nM) are incubated in one syringe while either buffer (panels A-C) or α-casein (20 μM) (panels D-F) are incubated in the other syringe of a stopped-flow fluorimeter at 25 °C. The contents of the two syringes are rapidly mixed. Fluorescence is excited at 494 nm and emission is observed at 515 nm and above. Time courses are shown in solid blue lines. Fits of each time course to a single exponential are shown in dashed black lines. The rate constants were determined to be (A) $(0.0038 \pm 0.0001)\ s^{-1}$, (B) $(0.00157 \pm 0.00005)\ s^{-1}$, (C) $(0.0025 \pm 0.0002)\ s^{-1}$, (D) $(0.0054 \pm 0.0001)\ s^{-1}$, (E) $(0.0025 \pm 0.0002)\ s^{-1}$, (F) $(0.00425 \pm 0.00003)\ s^{-1}$, and (G) $(0.00453 \pm 0.00004)\ s^{-1}$, where reported errors are the standard deviation from 1,000 iterations of Monte Carlo simulations.

Supplementary Figure 4. Analysis of Hsp104 anisotropy time courses. Representative time courses of Hsp104 translocation and dissociation from N-terminally labeled 102 and 127 amino acid truncations of αS1-casein. Experiments were carried out as shown in Figure 1B with 2 μM Hsp104, 300 μM ATPγS and 100 nM α-casein 102 or 127 in one syringe and rapidly mixed with 10 mM ATP and 20 μM α-casein to serve as a trap for any unbound Hsp104. Fluorescence is excited using polarized light at 494 nm and fluorescence anisotropy and total fluorescence is simultaneously detected at 515 nm and above using a T format polarization accessory. Panel A and B show anisotropy as a function of time for α-casein 102 and 127, respectively along with a time course that represents the anisotropy of each α-casein truncation peptide alone. Panel C and D show the total fluorescence time courses for Hspp104 dissociation from α-casein 102 or 127 simultaneously collected with the anisotropy time courses in Panels A and B. The black dashed line represents the result of the nonlinear least squares analysis to Scheme 3. The best fit parameters for α-casein 102 are $k_{np} = (0.0037 \pm 0.0002)\ s^{-1}$, $k_{obs,1} = (26.3 \pm 0.4)\ s^{-1}$, $k_{obs,2} = (0.0564 \pm 0.0009)\ s^{-1}$, $x = 0.60 \pm 0.03$, $r_{c*} = 0.149 \pm 0.005$, $r_C = 0.147 \pm 0.005$, $r_I = 0.144 \pm 0.003$, $r_P = 0.114 \pm 0.002$, $q_{C*} = 4.52 \pm 0.01$, $q_C = 4.23 \pm 0.02$, $q_I = 4.34 \pm 0.01$, $q_P = 4.599 \pm 0.003$ and the best fit parameters for a-casein 127 are $k_{np} = (0.0045 \pm 0.0003)\ s^{-1}$, $k_{obs,1} = (0.471 \pm 0.007)\ s^{-1}$, $k_{obs,2} = (0.0441 \pm 0.0007)\ s^{-1}$, $x = 0.68 \pm 0.03$, $r_{c*} = 0.165 \pm 0.006$, $r_C = 0.17 \pm 0.006$, $r_I = 0.174 \pm 0.004$, $r_P = 0.147 \pm 0.002$, $q_{C*} = 4.98 \pm 0.01$, $q_C = 4.77 \pm 0.02$, $q_I = 4.72 \pm 0.02$, $q_P = 5.023 \pm 0.003$.

Supplementary Figure 5. Processive translocase anisotropy time course. (A) Representative time courses of ClpA translocation and dissociation from N-terminally labeled 102 (orange trace) and 127 (red trace) amino acid truncations of αS1-casein. ClpA (2 μM), ATPγS (300 μM), and fluorescein labeled casein substrate (20 nM) are incubated in one syringe, while ATP (10 mM) and α-casein (20 μM) are incubated in the other syringe of a stopped-flow fluorimeter at 25 °C. The contents of the two syringes are rapidly mixed. Fluorescence is excited using polarized light at 494 nm and fluorescence anisotropy is observed at 515 nm and above using a T format polarization accessory.

Supplementary Figure 6. Hsp104 does not exhibit a directional preference. (A) Time courses of Hsp104 translocation and dissociation from C-terminally labeled 30, 40, and 50 amino acid truncations of the RepA peptide were fit to the equation derived from Scheme 1. In green markers, the number of steps, *n,* is plotted as a function of polypeptide length, *l,* with the corresponding data from N-labeled peptides shown in gray for comparison. (B) In green, a representative anisotropy time course of Hsp104 translocation and dissociation from C-terminally labeled 127 amino acid truncation of αS1-casein is overlaid with the time course obtained from the N-terminally labeled 127 amino acid truncation in gray.

Figure 7. Residuals for Fit Describing ATP dependence of Hsp104 catalyzed polypeptide translocation. Representative ATP dependent Hsp104-catalyzed polypeptide translocation time courses (top) and the residulas from the fit of these data to Scheme 2 (bottom) are presented. Each color corresponds to a different ATP concentration, with 10 μM ATP shown in red. Intermediate concentrations of ATP go through orange, green, and blue, with the highest concentration, 5 mM ATP, shown in purple. The ATP concentrations that fall within the range of ATP:ATPγS that enhance Hsp104 activity are denoted by a gray asterisk. The data were fit to the equation derived from Scheme 2 using NLLS analysis

Supplementary Figure 8. Effect of ATP:ATPγS ratio on Hsp104 polypeptide translocation. Hsp104 (2 μM), ATPγS (variable), and fluorescently labeled RepA truncation peptide (20 nM) are incubated in one syringe, while ATP (variable) and α-casein (20 μM) are incubated in the other syringe of a stopped-flow fluorimeter at 25 °C. The contents of the two syringes are rapidly mixed. Fluorescence is excited at 494 nm and emission is observed at 515 nm and above. (A) Comparison of time courses collected with 3 mM ATP and differing concentrations of ATPγS. (B) Comparison of time courses collected with the same total nucleotide concentration (850 μM) and differing ratios of ATP:ATPγS. In both panels, the pink solid traces are from our standard nucleotide experimental conditions (as shown in Figure 3 in the main text) and the purple solid traces use the 3:1 ratio of ATP:ATPγS. In all cases, the black broken lines are the best fits of each time course individually to Scheme 2.

Supplementary Tables

Supplementary Table 1. Kinetic parameters determined from individual NLLS fitting to Equation from Scheme 2 to time courses collected with varied [Hsp104] in saturating (5 mM) ATP

[Hsp104] (M)	x	k_{np} (s^{-1})	$k_{obs,1}$ (s^{-1})	$k_{obs,2}$ (s^{-1})
2.00E-07	0.59	0.01	0.088	0.466
1.00E-06	0.71	0.009	0.079	0.367
2.00E-06	0.75	0.009	0.076	0.517
4.00E-06	0.68	0.029	0.103	0.299

[Hsp104] is concentration before mixing. The peptide used is 20 nM (before mixing) $RepA_{1\text{-}50Flu.}$

Supplementary Table 2. Kinetic parameters determined from individual NLLS fitting to Equation from Scheme 1, C-terminally labeled substrates

peptide length (amino acids)	k_{np} (s^{-1})	x	k_t (s^{-1})	n (steps)
30	0.034 ± 0.003	0.751 ± 0.006	0.140 ± 0.005	1.54 ± 0.04
40	0.014 ± 0.001	0.761 ± 0.007	0.099 ± 0.003	1.38 ± 0.02
50	0.0080 ± 0.0004	0.67 ± 0.02	0.102 ± 0.002	1.32 ± 0.02

Supplementary Table 3. Kinetic Parameters determined from individual NLLS fitting to Equation from Scheme 2 to time courses with varied ATP:ATPγS concentrations and ratios

Condition	[ATP]	[ATPγS]	[nucleotide]	k_{np} (s^{-1})	x	$k_{obs,1}$ (s^{-1})	$k_{obs,2}$ (s^{-1})
Standard	3.0E-3	150.0E-6	3.2E-3	0.009 ± 0.001	0.78 ± 0.04	0.095 ± 0.006	0.40 ± 0.04
Optimum	3.0E-3	1.0E-3	4.0E-3	0.005	0.46	0.050	0.217
Standard	700.0E-6	150.0E-6	850.0E-6	0.014 ± 0.004	0.75 ± 0.03	0.072 ± 0.004	0.19 ± 0.02
Optimum	637.5E-6	212.5E-6	850.0E-6	0.010	0.72	0.061	0.15

References

[1] Rajendar, B., and Lucius, A. L. (2010) Molecular mechanism of polypeptide translocation catalyzed by the Escherichia coli ClpA protein translocase, *J Mol Biol 399*, 665-679.

[2] Miller, J. M., Lin, J., Li, T., and Lucius, A. L. (2013) E. coli ClpA Catalyzed Polypeptide Translocation is Allosterically Controlled by the Protease ClpP, *Journal of Molecular Biology 425*, 2795-2812.

[3] Li, T., Weaver, C. L., Lin, J., Duran, E. C., Miller, J. M., and Lucius, A. L. (2015) Escherichia coli ClpB is a non-processive polypeptide translocase, *The Biochemical journal 470*, 39-52.

[4] Weaver, C. L., Duran, E. C., Mack, K. L., Lin, J., Jackrel, M. E., Sweeny, E. A., Shorter, J., and Lucius, A. L. (2017) Avidity for Polypeptide Binding by Nucleotide-Bound Hsp104 Structures, *Biochemistry 56*, 2071-2075.

[5] Doyle, S. M., Shorter, J., Zolkiewski, M., Hoskins, J. R., Lindquist, S., and Wickner, S. (2007) Asymmetric deceleration of ClpB or Hsp104 ATPase activity unleashes protein-remodeling activity, *Nature structural & molecular biology 14*, 114-122.

[6] Li, T., Lin, J., and Lucius, A. L. (2015) Examination of polypeptide substrate specificity for Escherichia coli ClpB, *Proteins 83*, 117-134.

[7] Fischer, C. J., and Lohman, T. M. (2004) ATP-dependent translocation of proteins along single-stranded DNA: models and methods of analysis of pre-steady state kinetics, *J Mol Biol 344*, 1265-1286.

[8] Williams, D. J., and Hall, K. B. (2000) Monte Carlo applications to thermal and chemical denaturation experiments of nucleic acids and proteins, *Methods Enzymol 321*, 330-352.

[9] Lucius, A. L., Maluf, N. K., Fischer, C. J., and Lohman, T. M. (2003) General methods for analysis of sequential "n-step" kinetic mechanisms: application to single turnover kinetics of helicase-catalyzed DNA unwinding, *Biophys J 85*, 2224-2239.

[10] Gates, S. N., Yokom, A. L., Lin, J., Jackrel, M. E., Rizo, A. N., Kendsersky, N. M., Buell, C. E., Sweeny, E. A., Mack, K. L., Chuang, E., Torrente, M. P., Su, M., Shorter, J., and Southworth, D. R. (2017) Ratchet-like polypeptide translocation mechanism of the AAA+ disaggregase Hsp104, *Science 357*, 273-279.

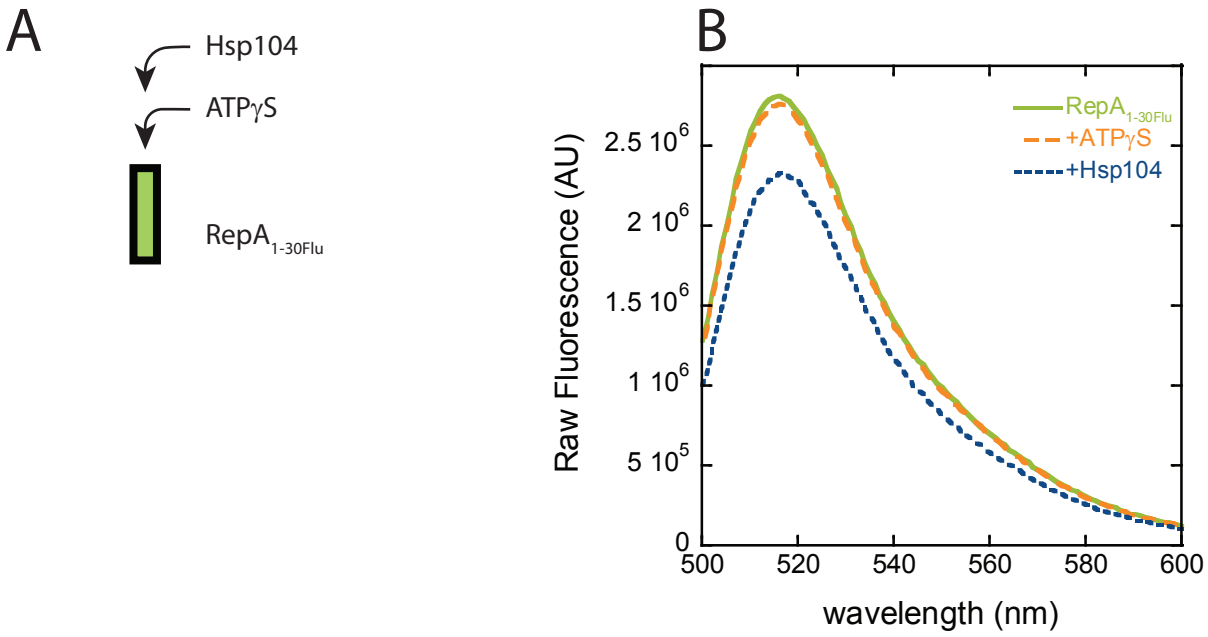

Supplementary Figure 1

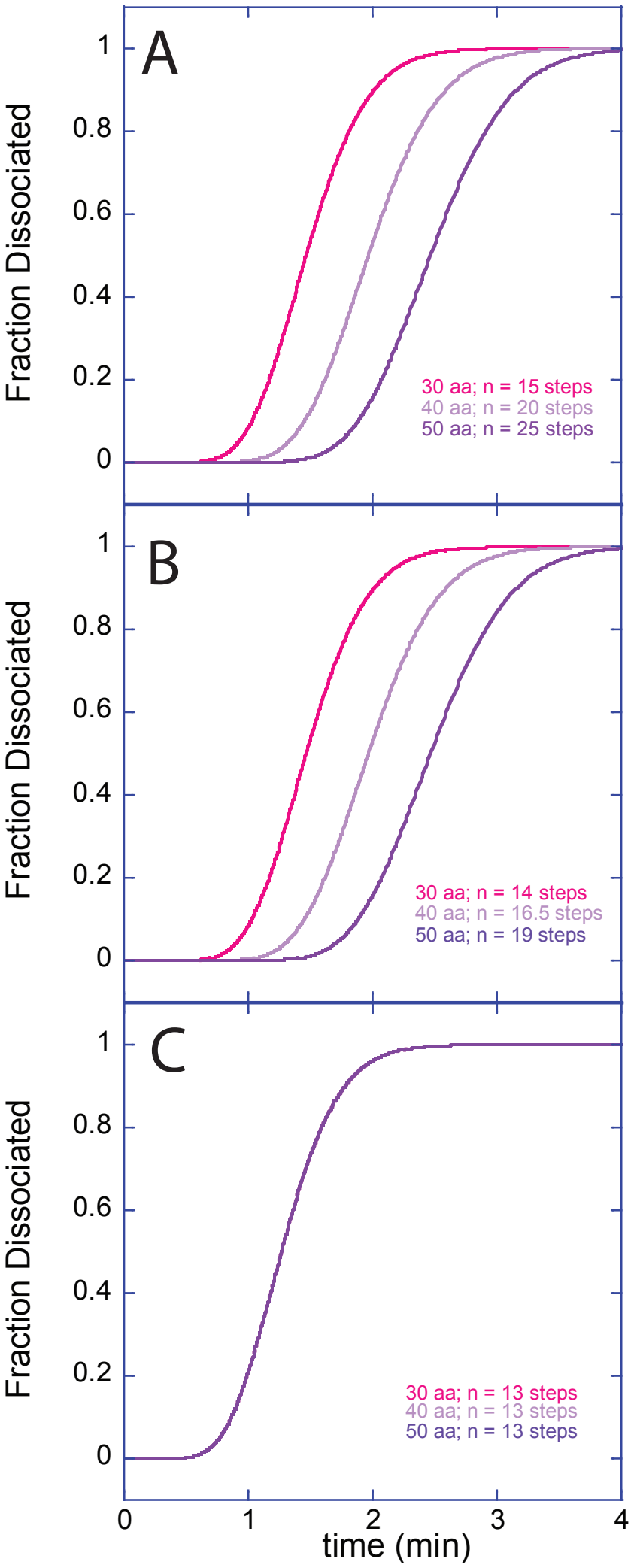

Supplementary Figure 2

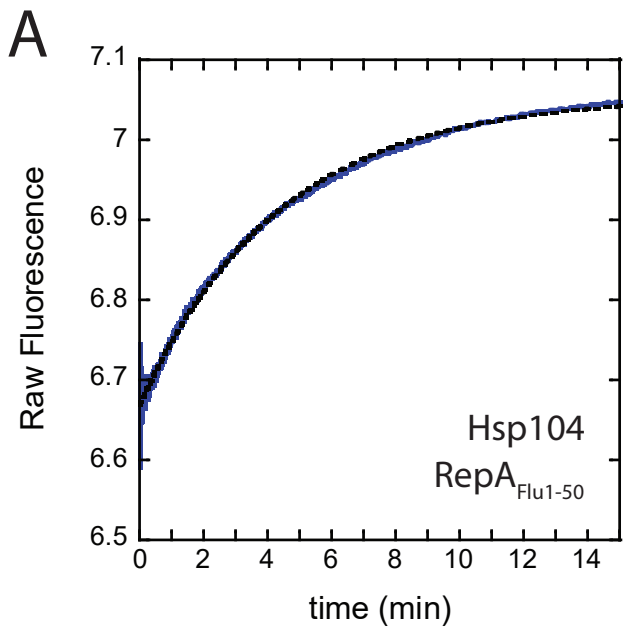

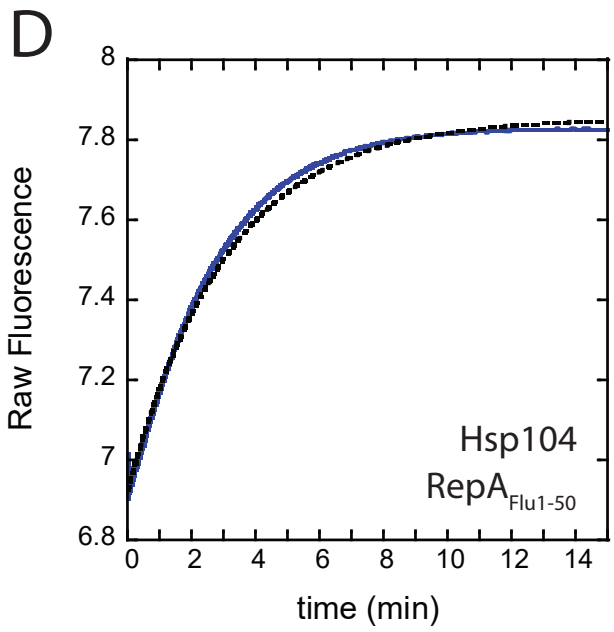

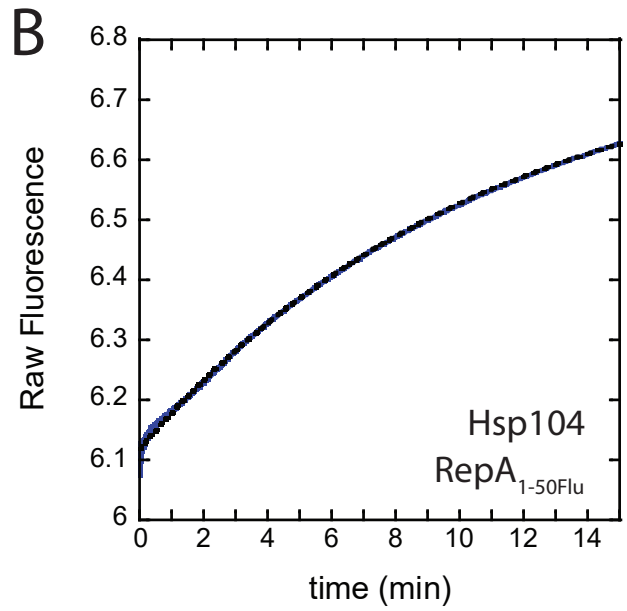

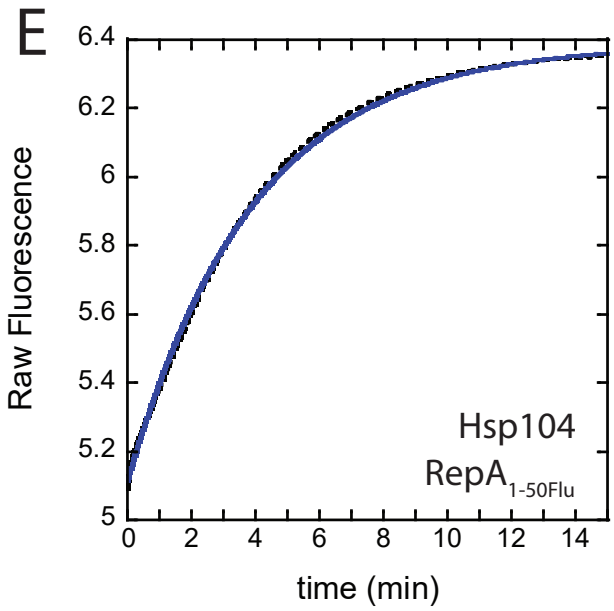

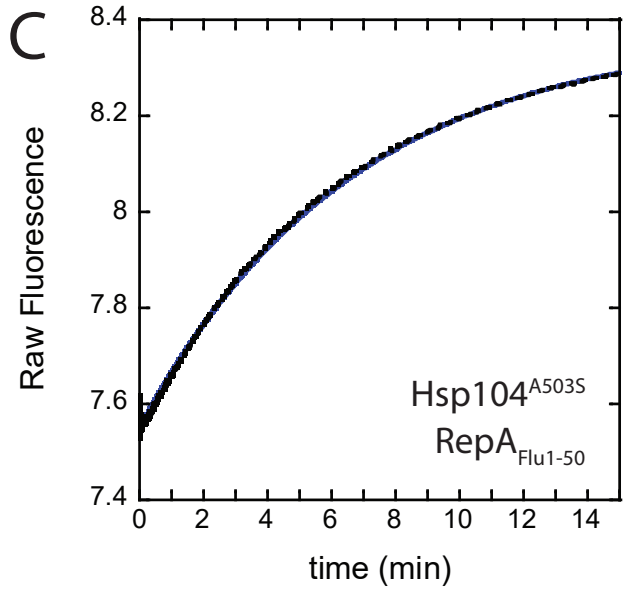

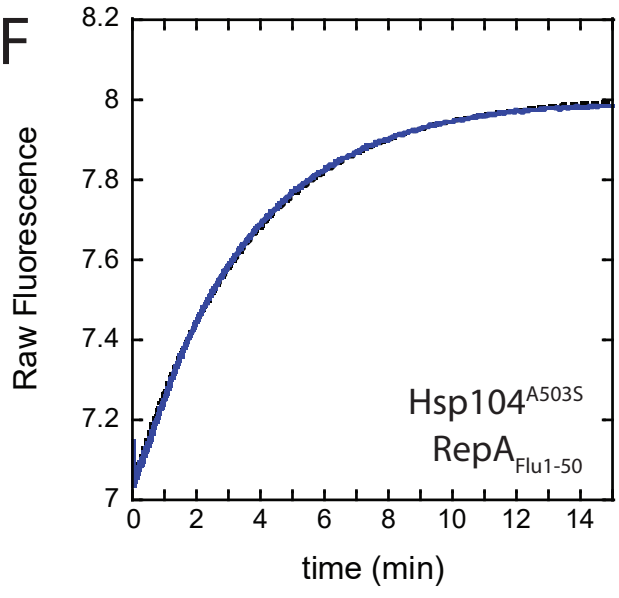

Supplementary Figure 3

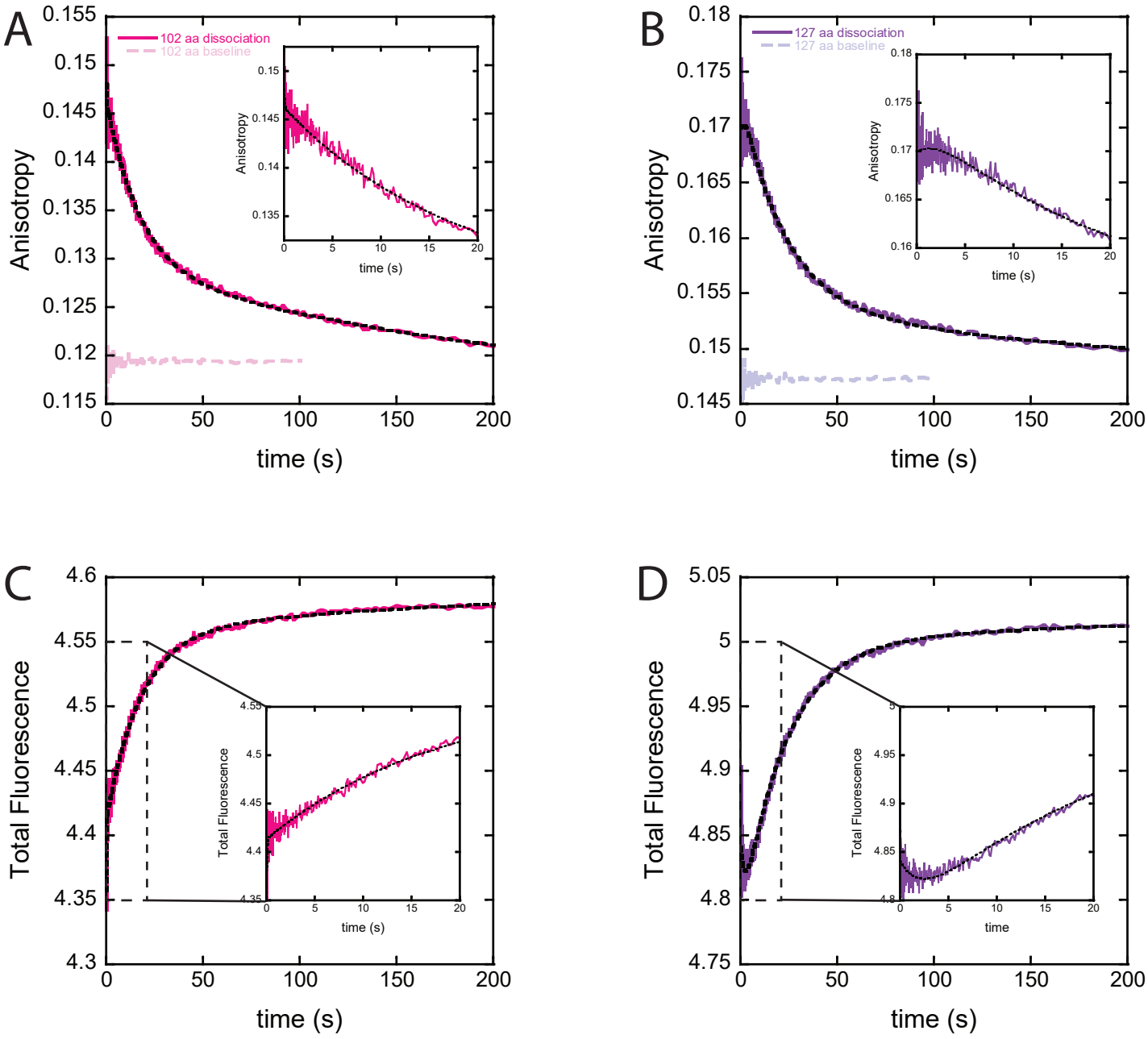

Supplementary Figure 4

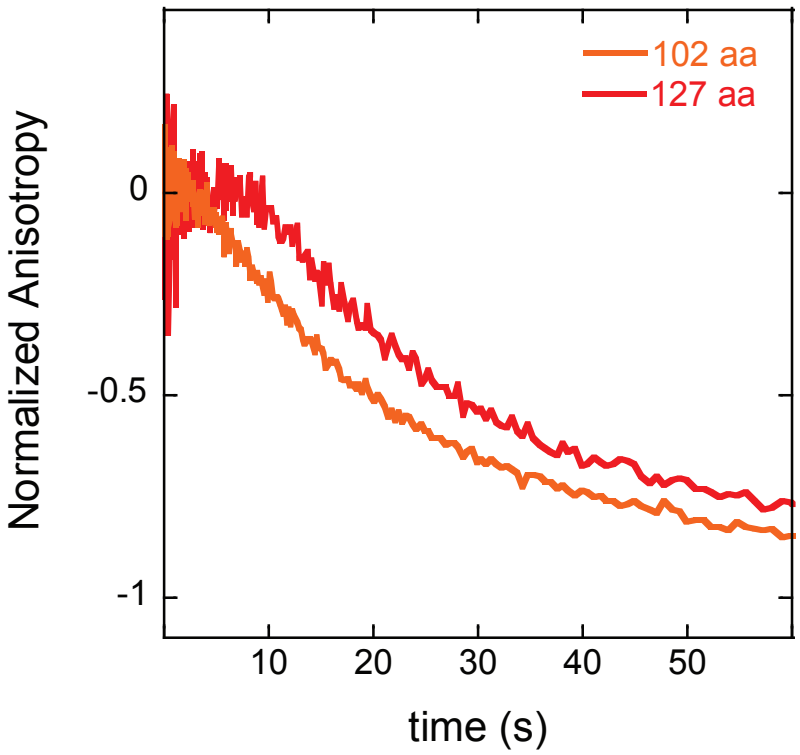

Supplementary Figure 5

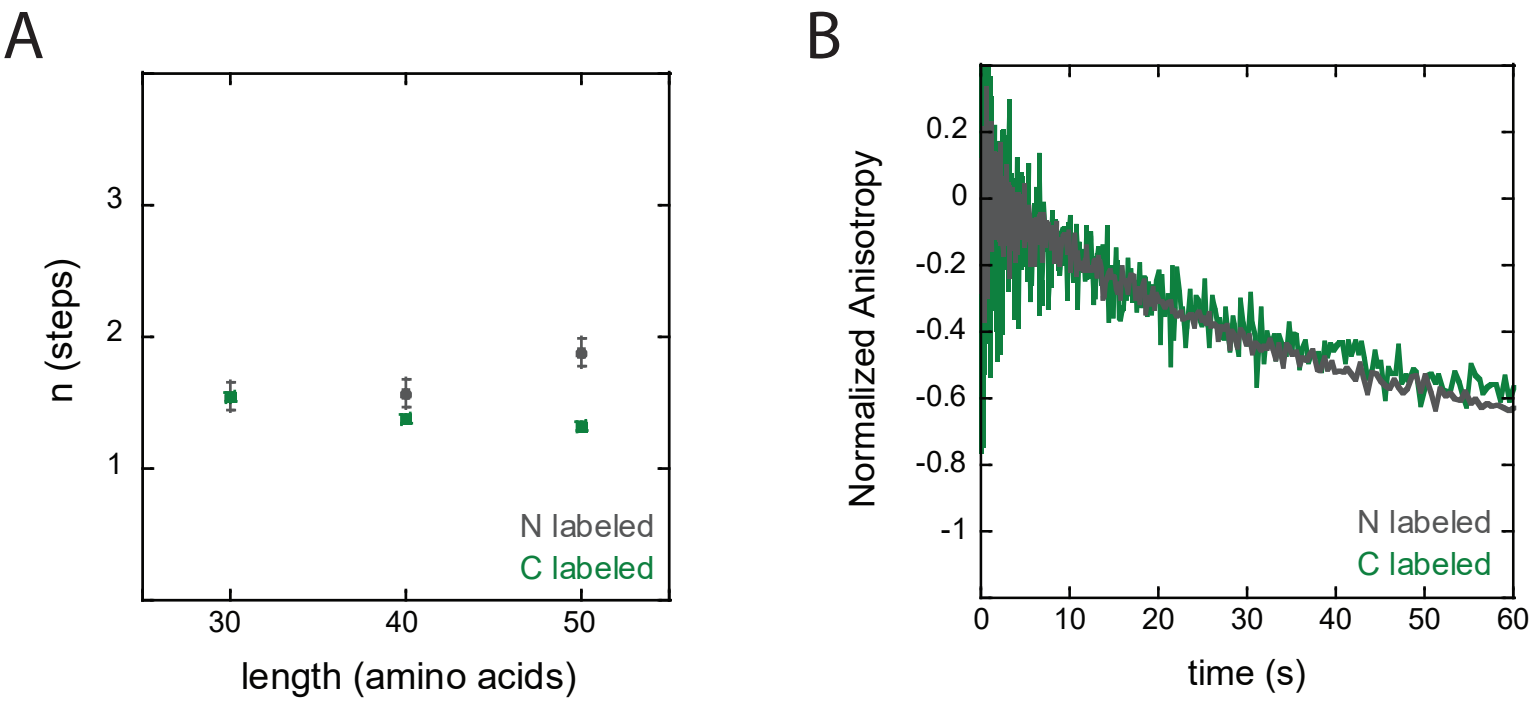

Supplementary Figure 6

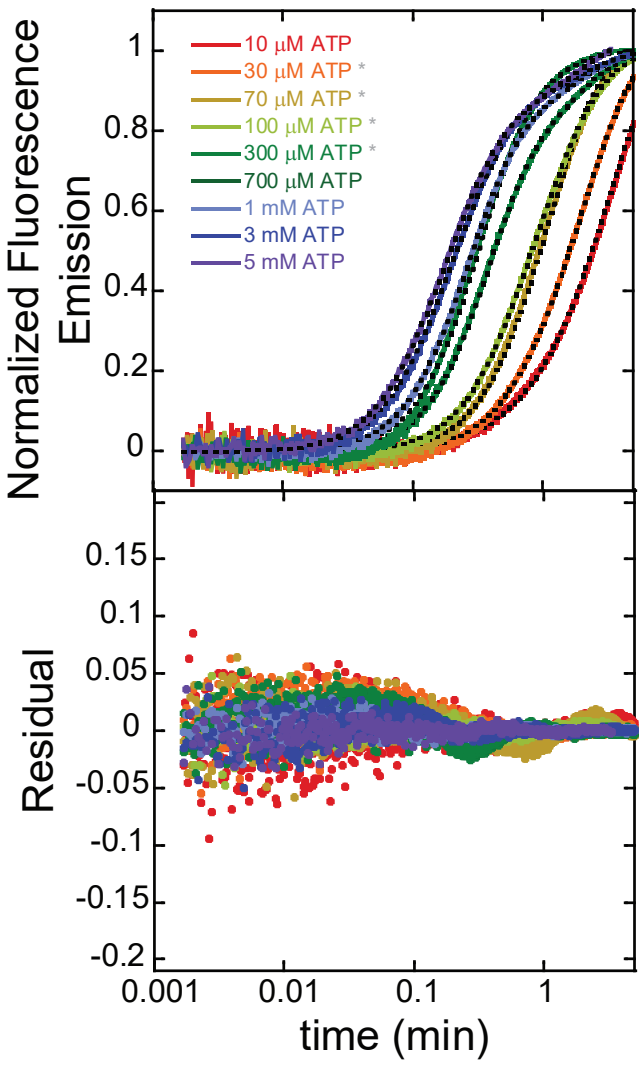

Supplementary Figure 7

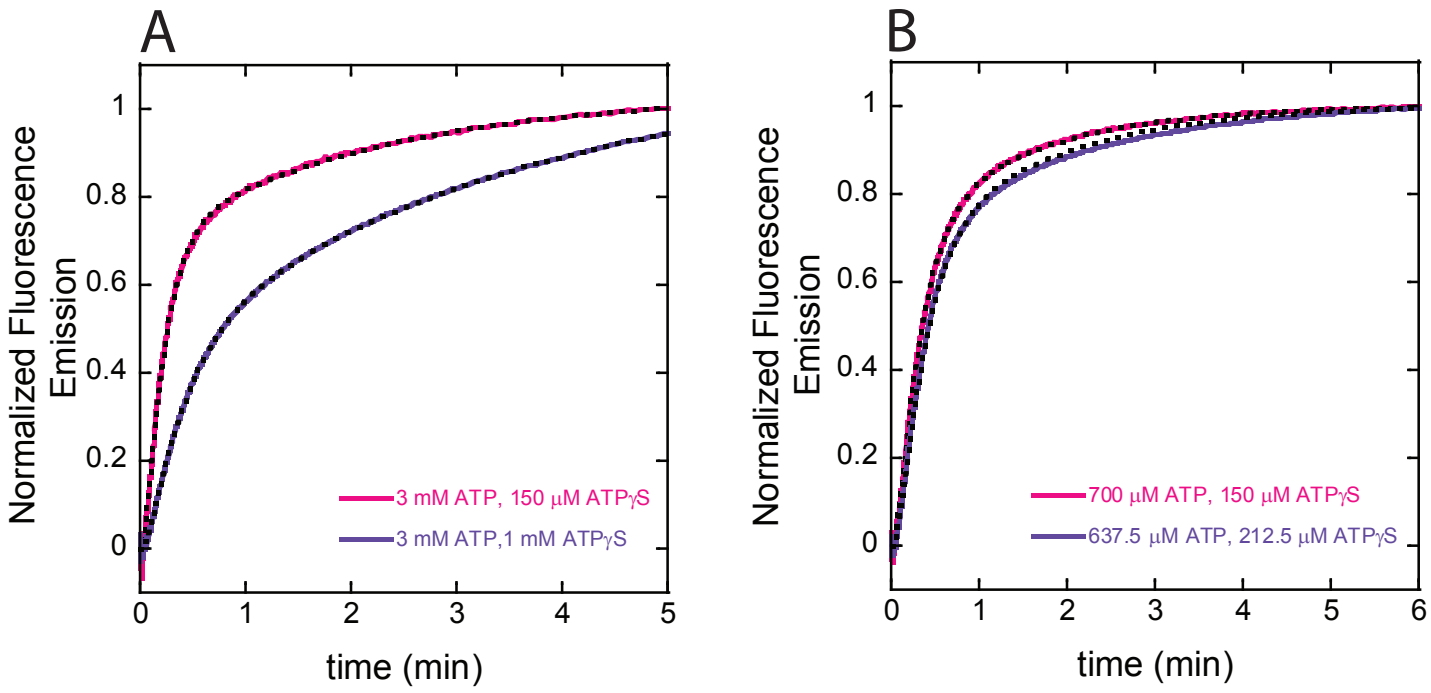

Supplemental Figure 8